Biophysical Journal
Article

Biophysical Society

Concise Whole-Cell Modeling of BK_{Ca}-CaV Activity Controlled by Local Coupling and Stoichiometry

Francesco Montefusco,[1] Alessia Tagliavini,[1] Marco Ferrante,[2] and Morten Gram Pedersen[1,*]
[1]Department of Information Engineering and [2]Department of Mathematics "Tullio Levi-Civita", University of Padua, Padua, Italy

ABSTRACT Large-conductance Ca^{2+}-dependent K^+ (BK_{Ca}) channels are important regulators of electrical activity. These channels colocalize and form ion channel complexes with voltage-dependent Ca^{2+} (CaV) channels. Recent stochastic simulations of the BK_{Ca}-CaV complex with 1:1 stoichiometry have given important insight into the local control of BK_{Ca} channels by fluctuating nanodomains of Ca^{2+}. However, such Monte Carlo simulations are computationally expensive, and are therefore not suitable for large-scale simulations of cellular electrical activity. In this work we extend the stochastic model to more realistic BK_{Ca}-CaV complexes with 1:*n* stoichiometry, and analyze the single-complex model with Markov chain theory. From the description of a single BK_{Ca}-CaV complex, using arguments based on timescale analysis, we derive a concise model of whole-cell BK_{Ca} currents, which can readily be analyzed and inserted into models of cellular electrical activity. We illustrate the usefulness of our results by inserting our BK_{Ca} description into previously published whole-cell models, and perform simulations of electrical activity in various cell types, which show that BK_{Ca}-CaV stoichiometry can affect whole-cell behavior substantially. Our work provides a simple formulation for the whole-cell BK_{Ca} current that respects local interactions in BK_{Ca}-CaV complexes, and indicates how local-global coupling of ion channels may affect cell behavior.

INTRODUCTION

Mathematical modeling has played an important role in investigations of cellular electrophysiology at least since the works on neuronal action-potential generation by Hodgkin and Huxley (1). In the Hodgkin-Huxley model and most of its descendants, the system of ion channels is coupled globally via the membrane potential or the bulk cytosolic Ca^{2+} concentration. However, some ion channels are colocalized, implying that the activity of one channel may affect the other via local control. Electrical activity is thus a result of the complex interactions of local and global coupling of ion channels. Of note, the standard Hodgkin-Huxley formulation does not take into account local coupling of channels.

Large-conductance Ca^{2+}- and voltage-dependent K^+ (BK_{Ca}, KCa1.1) channels, ubiquitously found in excitable cells where they shape electrical activity (2), provide an example of such ion channels, whose activity is influenced locally by associated voltage-gated Ca^{2+} channels (CaVs). BK_{Ca} channels have a single-channel conductance of ~100 pS in physiological conditions (3), and are activated by Ca^{2+} and transmembrane voltage, which is seen as a Ca^{2+}-dependent left-shift of the BK_{Ca} activation curve (4–6). In neurons (7–10) and vascular myocytes (11), BK_{Ca} channels colocalize with CaVs, which exposes the BK_{Ca} channels to the Ca^{2+} nanodomains below the mouth of the CaV channels (12–15), where the local Ca^{2+} concentration reaches the tens of micromolar that are required for activating the BK_{Ca} channels at physiological voltages (2,16). There is increasing evidence for a direct coupling between BK_{Ca} and CaV channels, forming BK_{Ca}-CaV ion channel complexes with a stoichiometry of 1–4 CaV channels per BK_{Ca} channel (2,11), and differences in stoichiometry likely affect channel activity. Intuitively, we expect that more CaVs per complex would augment the BK_{Ca} open probability, both because of higher local Ca^{2+} concentration when the CaVs open simultaneously, and because of greater probability that at least one of the CaVs is open at any given time.

Recently, Cox (17) presented a Markov chain model for a BK_{Ca}-CaV complex with 1:1 stoichiometry, and performed Monte Carlo simulations that provided important insight into the open probability of BK_{Ca} channels during depolarizations and action potentials, and how e.g., inactivation of CaVs directly influence BK_{Ca} channel activity. Such Monte Carlo simulations are computationally intensive and explicit mathematical relations between assumptions and consequences

Submitted February 14, 2017, and accepted for publication April 25, 2017.
*Correspondence: pedersen@dei.unipd.it
Editor: Arthur Sherman.
http://dx.doi.org/10.1016/j.bpj.2017.04.035

are not available. Monte Carlo simulations have also been performed for whole-cell simulations of electrical activity to investigate the effects of stochastic ion channel kinetics, for example for Ca^{2+}-sensitive SK and BK_{Ca} channels controlled by local Ca^{2+} dynamics (18,19). When stochasticity is not of interest, to speed up simulations, many models of whole-cell electrical activity that include BK_{Ca} channels express this current in a simplified way that neglects local effects due to the BK_{Ca}-CaV complexes (20,21) or use heuristic expressions involving the whole-cell Ca^{2+} currents (22,23), which may not respect the dynamics within BK_{Ca}-CaV complexes. Alternatively, diffusion of Ca^{2+} around a CaV (or a cluster of synchronized CaVs) has been simulated to investigate, e.g., how BK channels inherit properties of the CaVs, and how distance between channels influence BK_{Ca} activity (10). Another frequent approach (which, however, neglects local interactions) is to model Ca^{2+} dynamics in one or more shells beneath the cell membrane, which then drives BK_{Ca} channels (24–26). The computational intensity is increased in such a model because local Ca^{2+} concentrations resulting from buffering and diffusion must be simulated in addition to ion channel gating.

It would therefore be advantageous to have a simple but mechanistically correct model of the BK_{Ca} current, which respects the local effects of BK_{Ca}-CaV coupling, and that can be inserted in Hodgkin-Huxley-type models of whole-cell electrical activity. Such a model would also make explicit how local effects and stochastic ion channel kinetics are reflected in average, whole-cell behavior of BK_{Ca} channels with the advantage compared to simulations that the dependence on parameters can be read directly from the formulas of the reduced model. Here we achieve both these aims. Our approach is similar to analyses of Ca^{2+}-dependent inactivation of Ca^{2+} channels (27), and local control of ryanodine receptors in dyadic subspaces (28,29). Importantly, in the nanodomains controlling BK_{Ca} activity, Ca^{2+} is fast enough to avoid the need for, e.g., a probability-density approach for handling local Ca^{2+} dynamics correctly at the whole-cell level (30). We use the mechanistically correct description of single BK_{Ca}-CaV complexes with 1:1 stoichiometry developed by Cox (17) as the natural starting point for constructing a reduced model for BK_{Ca}-CaV complexes with 1:n stoichiometry to be inserted into a whole-cell model of electrical activity. Our results give insight into the simulations of single BK_{Ca}-CaV complexes, and clarify that it is the local effects of ion channel kinetics rather than stochasticity per se that determine whole-cell activity.

MATERIALS AND METHODS

BK_{Ca} channel model

We describe the BK_{Ca} channel with a model of single-channel gating with two states (closed and open). Fig. S1 *A* shows a schematic representation of the model, where X corresponds to the closed state and Y to the open state.

The mathematical description of BK_{Ca} voltage- and calcium-dependent activation is given by the following:

$$\frac{dp_Y}{dt} = -k^- p_Y + k^+(1-p_Y), \tag{1}$$

where p_Y represents the open probability for the BK_{Ca} channel, and k^- and k^+ are the voltage- and calcium-dependent rate constants. As shown in the Supporting Material, from relatively mild assumptions and experimental evidence, we can express these rates as the following:

$$k^- = w^-(V)f^-(Ca), \tag{2}$$

$$k^+ = w^+(V)f^+(Ca), \tag{3}$$

where Ca denotes the Ca^{2+} concentration at the BK_{Ca} channels. At fixed Ca^{2+} levels, BK_{Ca} activation is well described by Boltzmann functions (6,8,16). Hence, we assume that the voltage-dependent rate constants, w^-, for the transition from the open to closed state, and w^+, for the transition from the closed to open state, have the following standard forms:

$$w^-(V) = w_0^- e^{-w_{yx}V}, \tag{4}$$

$$w^+(V) = w_0^+ e^{-w_{xy}V}, \tag{5}$$

where the parameters $w^-{}_0$ and $w^+{}_0$ are voltage-independent.

There is evidence that at fixed V, Ca^{2+} stabilizes the open state (4), i.e., f^- should decrease with Ca, and that >1 Ca^{2+} ion is needed for BK_{Ca} activation, which is a sigmoidal function of the Ca^{2+} concentration (4,16). The calcium-dependent relations are therefore modeled by the following:

$$f^-(Ca) = 1 - \frac{Ca^{n_{yx}}}{K_{yx}^{n_{yx}} + Ca^{n_{yx}}} = \frac{1}{1+\left(\frac{Ca}{K_{yx}}\right)^{n_{yx}}}, \tag{6}$$

$$f^+(Ca) = \frac{Ca^{n_{xy}}}{K_{xy}^{n_{xy}} + Ca^{n_{xy}}} = \frac{1}{1+\left(\frac{K_{xy}}{Ca}\right)^{n_{xy}}}, \tag{7}$$

where K_{yx} and K_{xy} are the calcium affinities when the channel closes and opens, respectively, and n_{yx} and n_{xy} are the corresponding Hill coefficients. By using the relationships in Eqs. 4–7, we get the following formulas for the equilibrium open fraction of BK_{Ca} channel activation, p_{Y_∞}, and the corresponding time constant τ_{p_Y}:

$$p_{Y_\infty} = \frac{k^+}{k^- + k^+} = \frac{1}{1 - e^{-\frac{V-V_0}{S_0}}}, \tag{8}$$

$$\tau_{p_Y} = \frac{1}{k^- + k^+} = \frac{e^{w_{xy}V}}{w_0^+}\left(1+\left(\frac{K_{xy}}{Ca}\right)^{n_{xy}}\right)\frac{1}{1-e^{-\frac{V-V_0}{S_0}}}, \tag{9}$$

where

$$V_0 = \left(\log\frac{w_0^-}{w_0^+} + \log\left(1+\left(\frac{K_{xy}}{Ca}\right)^{n_{xy}}\right) - \log\left(1+\left(\frac{Ca}{K_{yx}}\right)^{n_{yx}}\right)\right)S_0, \tag{10}$$

$$S_0 = \frac{1}{w_{yx} - w_{xy}}. \tag{11}$$

We use global optimization to estimate the model parameters providing the best fit to the experimental data (17), consisting of BK_{Ca} open probabilities and time constants as functions of voltage, at different Ca^{2+} concentrations. In particular, we formulate an optimization problem to minimize the sum of the squared errors between the simulated responses produced by the model and the corresponding experimental data as follows:

$$\min_{\theta} J = \sum_j \sum_i \left(p_{Y_{\infty_j}}(V_i) - \widehat{p}_{Y_{\infty_j}}(V_i, \theta) \right)^2 + \left(\tau_{p_{Yj}}(V_i) - \widehat{\tau}_{p_{Yj}}(V_i, \theta) \right)^2, \tag{12}$$

where θ is the set of model parameters, and $p_{Y_{\infty_j}}(V_i)$ and $\tau_{p_{Yj}}(V_i)$ are the experimental BK_{Ca} steady-state open fraction and corresponding time constants, respectively, at the given voltage V_i for the jth experiment (corresponding to a given Ca^{2+} concentration). $\widehat{p}_{Y_{\infty_j}}(V_i, \theta)$ and $\widehat{\tau}_{p_{Yj}}(V_i, \theta)$ are the simulated equilibrium open fraction of the BK_{Ca} channel and the corresponding time constants of the model, respectively, at the given V_i for the jth experiment. For the optimization, we use a hybrid genetic algorithm (GA) (31) that combines the most well-known type of evolutionary algorithm with a local gradient-based algorithm (32). We use the function "ga" from the software MATLAB (The MathWorks, Natick, MA) Global Optimization Toolbox and fmincon from the MATLAB Optimization Toolbox as the local algorithm. We repeat the hybrid GA algorithm several times and select the parameter set that gives the best fitting. Table S1 reports the optimal model parameters, and Fig. S1, *B–G* shows the fits to the data.

CaV channel model

We describe the calcium channel dynamics with the following model (27):

$$\frac{dc}{dt} = \beta o - \alpha c, \tag{13}$$

$$\frac{do}{dt} = \alpha c + \gamma b - (\beta + \delta) o, \tag{14}$$

$$b = 1 - c - o = 1 - h, \tag{15}$$

where c corresponds to the closed state, o to the open state, and b to the inactivated (blocked) state of the calcium channel; h represents the fraction of Ca^{2+}channels not inactivated, δ is the rate for channel inactivation, and γ is the reverse reactivation rate; and α and β represent the voltage-dependent Ca^{2+} channel opening rate and closing rate, respectively, and have the following forms:

$$\alpha(V) = \alpha_0 e^{-\alpha_1 V}, \tag{16}$$

$$\beta(V) = \rho\left(\beta_0 e^{-\beta_1 V} + \alpha_0 e^{-\alpha_1 V}\right). \tag{17}$$

As shown in Sherman et al. (27), the processes of activation and inactivation can be approximately separated in time, because activation is much faster than inactivation. In particular, we achieve the following model for the activation variable, m_{CaV},

$$\frac{dm_{CaV}}{dt} = \frac{m_{CaV,\infty} - m_{CaV}}{\tau_{CaV}}, \tag{18}$$

where

$$m_{CaV,\infty} = \frac{\alpha}{\alpha + \beta}, \quad \tau_{CaV} = \frac{1}{\alpha + \beta}, \tag{19}$$

and the following equation for inactivation:

$$\frac{db}{dt} = m_{CaV,\infty}\,\delta - (m_{CaV,\infty}\,\delta + \gamma) b. \tag{20}$$

As for the BK_{Ca} channel, we use a global optimization method to optimize the parameters of Eqs. 16 and 17 to fit the experimental data presented by Cox (17), i.e., peak open probabilities and time constants as functions of voltage. For the values of $\gamma = 0.0020\ ms^{-1}$ and $\delta = 0.0025\ \mu M^{-1}\ ms^{-1} \times [Ca_{CaV}]$, we use those reported by Cox (17). Ca_{CaV} is the Ca^{2+} concentration at the internal mouth of the channel and defined by Eq. S1 with $r = 7$ nm, representing the distance of the sensor for Ca^{2+}-dependent inactivation from the channel pore. Note that the relation given by Eq. 17 allows scaling of the amount of channel activation at high voltage values according to the experiments (i.e., not all the calcium channels are open even for high voltages). Table S1 reports the optimal parameters for the CaV activation model.

BK_{Ca}-CaV complex with 1:1 and 1:*n* stoichiometries

Combining the models for BK_{Ca} and CaV channels, we obtain the models of the 1:1 (see Results and Supporting Material, Model of the 1:1 BK_{Ca}-CaV Complex and Timescale Analysis and Model Simplifications) and 1:*n* BK_{Ca}-CaV complexes (see Results and Supporting Material, Model for BK_{Ca} Activation in Complexes with k Noninactivated CaVs and its Approximation). Ca^{2+} levels sensed by the BK_{Ca} channel were assumed to reach steady state immediately after CaV opening or closure (17), and the steady-state Ca^{2+} concentration Ca_o resulting from influx through a single CaV was calculated by an explicit formula (see Eq. S1), assuming that CaV and BK_{Ca} channels are $r = 13$ nm apart (2,9). At $V = 0$ mV, $Ca_o \approx 19\ \mu M$ (see Supporting Material, Model of the 1:1 BK_{Ca}-CaV Complex and Table S2 for further details). In the case of more than one CaV per complex, the linear buffer approximation (33) was used to summarize Ca^{2+} levels when more than one CaV is open. We note that $k^+_c \approx 0$ (see Supporting Material, Model of the 1:1 BK_{Ca}-CaV Complex and Table S1) because the background Ca^{2+} concentration Ca_c is much below the levels needed for BK_{Ca} activation at physiological voltages (2). Thus, a BK_{Ca} channel opens only when a CaV in the complex is open. This approximation is used widely in our derivations, and is supported by the fact that Ca^{2+} influx via CaVs is needed to open BK_{Ca} channels (34), and that the submembrane Ca^{2+} concentration of some hundreds of nanomolar that a BK_{Ca} in a complex without open CaVs would sense, is too low to activate BK_{Ca} channels at physiological voltages (2,17).

We refer to the Supporting Material for details on mathematical analysis of the time to first BK_{Ca} channel opening using phase-type distributions (35) (see Supporting Material, Model of the 1:1 BK_{Ca}-CaV Complex), and timescale analysis used for model reduction borrowing ideas from enzyme kinetics (36) (see Supporting Material, Timescale Analysis and Model Simplifications and Model for BK_{Ca} Activation in Complexes with k Noninactivated CaVs and its Approximation), as well as for details on the whole-cell models investigated (see Supporting Material, Whole-Cell Models).

Availability of models and computer code

MATLAB code containing the files for generating the results presented in the main text and Supporting Material is provided as an additional Supporting File S1.

RESULTS

A simple Markov chain model of the BK_{Ca}-CaV complex

Cox (17) presented a stochastic model of a single CaV2.1 (P/Q-type) controlling a BK_{Ca} channel (α-subunits only) via local Ca^{2+}. The channels were located 13 nm apart, corresponding to physical coupling (2,9). The CaV was described by a seven-state Markov chain, and when the Ca^{2+} channel opened or closed, the local Ca^{2+} level was assumed to reach equilibrium instantaneously, in accordance with simulations of Ca^{2+} diffusion (12,13,17). The calculated local Ca^{2+} concentration was then assumed to drive a 10-state Markov chain model of the BK_{Ca} channel, and Monte Carlo simulations were performed.

We set out to simplify the description of the 7 × 10-state Markov chain model of the BK_{Ca}-CaV complex. This was achieved by assuming a three-state model for CaV (27) with states closed (*C*), open (*O*), or inactivated (*B*, for blocked) (see Materials and Methods). Parameters were adjusted to reproduce traces from Cox (17). The BK_{Ca} channel was represented by a model with only two states, closed (*X*) or open (*Y*) (see Materials and Methods). The transitions between states were supposed to depend on voltage and local Ca^{2+}, which was assumed to reach equilibrium instantaneously, and depend on voltage via the single-channel Ca^{2+}current (17). Parameters describing BK_{Ca} kinetics were fitted to data from Cox (17). Combining these two models, we obtain a six-state model of the BK_{Ca}-CaV complex (Fig. 1 *A*) that shows behavior similar to the 70-state model used by Cox (17) (Fig. 1, *B* and *C*). Our simplified BK_{Ca} model does not describe details of single-channel kinetics, which is not our scope here, but reproduces satisfactorily activation curves and times (Fig. S1), as well as whole-cell currents (Figs. S4 and S5), thus making it appropriate for analysis of whole-cell BK_{Ca} activity.

Time to first opening

Interestingly, Cox (17) found that not all simulated BK_{Ca} channels open during 20 ms depolarizations or imposed action potentials. We now study the time to the first opening of the BK_{Ca} channel during a depolarization, which mathematically corresponds to the first time the Markov chain *Z* corresponding to Fig. 1 *A* visits one of the states *CY*, *OY*, or *BY* starting from state *CX*. We denote the time to first opening $T_{CX,\psi}$, which is a random variable. Simulations show that eventually all BK_{Ca} channels open, and that the probability of channel opening before a given time *t*, $P(T_{CX,Y} < t)$, shows biphasic behavior (Fig. S2). Taking advantage of the fact that transitions from *CX* to *CY*, and from *BX* to *BY* have virtually zero probability (BK_{Ca} channels open only if the CaV is open), we obtain explicit formulas for the average time to first opening $E(T_{CX,Y})$ and, more generally, for the distribution function $P(T_{CX,Y} < t)$ using phase-type distribution results for Markov chains (35) (see Supporting Material, Time to First Opening and Phase-Type Distributions), as follows:

$$E(T_{CX,Y}) = \frac{1}{\alpha} + \frac{1}{k_o^+} + \frac{1}{k_o^+}\left(\frac{\beta}{\alpha} + \frac{\delta}{\gamma}\right), \tag{21}$$

$$P(T_{CX,Y} < t) = 1 - \sum_{\psi \in \{C,O,B\}} \left(\exp\left(t\overline{Q}\right)\right)_{CX,\psi X}, \tag{22}$$

where $\overline{Q}$ is the subtransition rate matrix of *Z* corresponding to states {*CX*, *OX*, *BX*}. Thus, the average time to first opening is inversely related to the opening rates of the CaV and

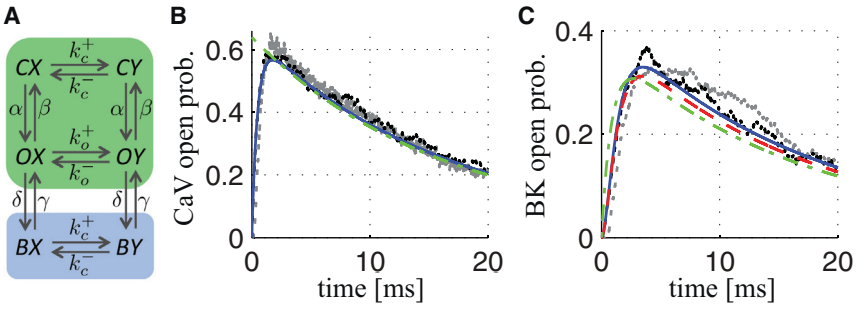

FIGURE 1 Six-state model of the BK_{Ca}-CaV complex with 1:1 stoichiometry and its simplification. (*A*) Shown here is a scheme indicating the six states and voltage-dependent transitions. *C*, *O*, and *B* refer respectively to closed, open, and inactivated states of the CaV, whereas *X* and *Y* indicate the closed and open states of the BK_{Ca} channel. The subscripts *o* and *c* on the horizontal transition rates indicate dependence on the Ca^{2+} concentration below an open (respectively, closed) Ca^{2+} channel. At physiological voltages, the transition to a state with an open BK_{Ca} channel occurs virtually only when the CaV is open ($k^+_c \approx 0$). The green box indicates states with noninactivated CaVs, whereas the blue box highlights states with inactivated CaVs. The transitions between the colored boxes are slow compared to transitions within boxes. (*B*) Shown here are simulated CaV open probabilities in response to a voltage step from −80 to 0 mV, obtained from the seven-state Markov chain model (*gray*; (17)), the three-state Markov chain model *C*, *O*, *B* (*black*; (27)), the ODE model corresponding to the three-state model (Eqs. 13–15; *blue*), and the corresponding model assuming instantaneous activation $m_{CaV} = m_{CaV,\infty}$ (Eq. 20; *dash-dotted green*). (*C*) Shown here are simulated open probabilities, in response to a voltage step from −80 to 0 mV, for BK_{Ca} channels controlled by CaVs in complexes with 1:1 stoichiometry, obtained from the original 70-state Markov chain model (*gray*; (17)), the six-state Markov chain model (*A*; *black*), the ODE model corresponding to the six-state model (Eqs. S6–S11; *blue*), the simplified Hodgkin-Huxley-type model (Eq. 25; *dashed red*), and the corresponding model assuming instantaneous activation $m_{CaV} = m_{CaV,\infty}$ (*dash-dotted green*; see main text). In (*B*) and (*C*), one-thousand realizations were simulated for the Markov chain models, and the average of these Monte Carlo simulations is shown. To see this figure in color, go online.

BK_{Ca}, and to the rate of reactivation after inactivation of the CaV. The involvement of these two processes explains the biphasic behavior, because escape from inactivation is much slower than channel opening. Eq. 22 states that $P(T_{CX,Y} < t)$ is 1 minus the probability of not having left $\{CX, OX, BX\}$ before t, and makes it explicit that ~15% of BK_{Ca} channels do not open during a 20 ms depolarization (17), because $P(T_{CX,Y} < 20\text{ ms}) \approx 85\%$ with our parameters (Fig. S2).

A concise deterministic model of cellular BK_{Ca} activity derived from multiscale principles

1:1 stoichiometry

For Hodgkin-Huxley-type whole-cell simulations, we do not need to know the state of each single BK_{Ca} channel, but it suffices to follow the BK_{Ca} open probability p_Y over time, because in the presence of many channels the whole-cell BK_{Ca} current is $I_{BK} = g_{BK}\, p_Y(V - V_K)$, where g_{BK} is the maximal whole-cell BK_{Ca} conductance and V_K is the K^+ reversal potential.

The time evolution of the probability distribution of the Markov chain Z corresponding to the six-state model in Fig. 1 *A* can be described by a system of five ordinary differential equations (ODEs) because the probabilities sum to 1. Denote, for $\psi \in \{C, O, B\}$ and $\xi \in \{X, Y\}$, the state probabilities $p_{\psi\xi}(t) = P(Z(t) = \psi\xi)$. Then $p_Y(t) = p_{CY}(t) + p_{OY}(t) + p_{BY}(t)$. As shown in Fig. 1 *C*, the average fraction of open channels calculated from Monte Carlo simulations of the Markov chain is well approximated by p_Y obtained from the ODE system.

Although the reduction to five ODEs for the description of the BK_{Ca}-CaV complexes is already a substantial reduction compared to Monte Carlo simulations, we wish to obtain an expression for the BK_{Ca} current of Hodgkin-Huxley form. Such a simplification provides further insight into the regulation of BK_{Ca} activity by CaVs, and provides the base for concise handling of BK_{Ca}-CaV complexes with 1:n stoichiometry.

We performed detailed timescale analysis (see Supporting Material, Timescale Analysis and Model Simplifications) based on the fact that re- and inactivation of CaVs are slower than (de-)activation. Thus, on a fast timescale, the average fraction of noninactivated CaVs, $h = 1 - (p_{BX} + p_{BY})$, is assumed to be constant, and the model splits into two submodels with, respectively, four and two states (Fig. 1 *A*, *green* and *blue*).

In the system of ODEs describing the state probabilities of the corresponding reduced four-state Markov chain (Fig. 1 *A*, *green*), it turns out that the dynamics of state CY is the fastest because CaV kinetics and BK_{Ca}-channel closure, when the CaV is closed, are faster reactions than BK_{Ca} gating in the presence of an open CaV (see Fig. S3). Assuming quasi-steady state for CY, we derive a single ODE describing the gating variable m_{BK}, which models the fraction of open BK_{Ca} channels in complexes with noninactivated CaV (see Supporting Material, Model Simplifications), as follows:

$$\frac{dm_{BK}}{dt} = \frac{m_{BK,\infty} - m_{BK}}{\tau_{BK}}, \tag{23}$$

with steady state and time constant given by the following:

$$\begin{aligned} m_{BK,\infty} &= \frac{m_{CaV}\, k_o^+ \left(\alpha + \beta + k_c^-\right)}{\left(k_o^+ + k_o^-\right)\left(k_c^- + \alpha\right) + \beta k_c^-}, \\ \tau_{BK} &= \frac{\alpha + \beta + k_c^-}{\left(k_o^+ + k_o^-\right)\left(k_c^- + \alpha\right) + \beta k_c^-}. \end{aligned} \tag{24}$$

Here, m_{CaV} is defined by Eq. 18 and denotes the activation variable for the CaV in the complex, which is routinely characterized in patch-clamp experiments and included in models of electrical activity via the time-constant, τ_{CaV}, and the steady-state activation function, $m_{CaV,\infty}$ (see Eq. 19). From these quantities, $\alpha = m_{CaV,\infty}/\tau_{CaV}$ and $\beta = 1/\tau_{CaV} - \alpha$ can be calculated. Note that Eq. 24 makes it explicit how $m_{BK,\infty}$ inherits properties of the associated Ca^{2+} channel type, as has been found experimentally (10,37).

Now, because BK_{Ca} channels close rapidly in complexes with inactivated CaVs (*blue* in Fig. 1 *A*), we have $p_Y \approx m_{BK}h$. Thus, the BK_{Ca} current is approximated by the standard Hodgkin-Huxley expression

$$I_{BK} = g_{BK} m_{BK} h (V - V_K), \tag{25}$$

where m_{BK} is given by Eq. 23, and h is the inactivation function of the CaVs (see Eqs. 15 and 20). As shown in Fig. 1 *C*, the open-probability expression $m_{BK}h$ approximates the Monte Carlo simulations very well. From Eq. 25 it is evident that the BK_{Ca} channels in BK_{Ca}-CaV complexes exhibit inactivation because of inactivation of the associated CaVs, and with approximately identical dynamics, as found in experiments (8) and Monte Carlo simulations (Fig. 1; (17)).

In many whole-cell models (e.g., (20–23)), the Ca^{2+} currents are assumed to activate instantaneously, which precludes calculation of α and β. Implicitly, such models assume that CaV gating is infinitely faster than the kinetics of other channels in the model. In our setting, this assumption corresponds to investigating the BK_{Ca}-CaV model defined by Eqs. 23–25 in the limit $\alpha, \beta \to \infty$. This leads to $\tau_{BK} \approx 1/[k_c^- - m_{CaV,\infty}(k_c^- - k_o^+ - k_o^-)]$ and $m_{BK,\infty} = k_o^+ m_{CaV,\infty} \tau_{BK}$, which are completely defined from BK_{Ca} kinetics and $m_{CaV,\infty}$. In combination with Eqs. 23 and 25, this model approximates the full system decently, except for the initial phase before CaV activation reaches equilibrium (Fig. 1 *C*, *green*). For whole-cell models

neglecting CaV activation kinetics, this initial-phase error should be of no more concern that the error in the Ca^{2+} current resulting from the steady-state assumption for CaV activation (Fig. 1 *B*, *green*).

Complexes with multiple Ca^{2+} channels

As mentioned, a BK_{Ca} channel can bind up to four CaVs (2,11). We extend our model to incorporate such cases, assuming that the n CaVs are all located 13 nm from the BK_{Ca} channel (2,9,17). Near the CaVs, the linear buffer approximation (33) holds, and the Ca^{2+} profile from n channels can be calculated by superimposing n nanodomains found for single, isolated CaVs.

One could in principle extend the Markov chain model in Fig. 1 *A* to a model with $3 \times n \times 2$ states. We take another approach to keep the model tractable. As discussed in the previous section, CaV inactivation is slow compared to other processes. We therefore assume that on a fast timescale, the fraction h of noninactivated CaVs is constant, and note that the BK_{Ca} channel closes rapidly when all CaVs in the complex are inactivated.

Consider a BK_{Ca}-CaV complex with $k \in \{1,..., n\}$ noninactivated CaVs. Neglecting inactivated CaVs, because they do not contribute to BK_{Ca} activation, such a complex can be described on the fast timescale by a Markov chain model with $2 \times (k + 1)$ states (Fig. 2 *A*). As for the case of 1:1 stoichiometry, we can approximate the dynamics of the BK_{Ca} open probability by a single ODE (see Supporting Material, Model for BK_{Ca} Activation in Complexes with k Noninactivated CaVs and its Approximation). Denote this open probability by $m_{BK}^{(k)}$, and note that $m_{BK}^{(1)} = m_{BK}$ in Eq. 23. Then, we have the following:

$$\frac{dm_{BK}^{(k)}}{dt} = \frac{m_{BK,\infty}^{(k)} - m_{BK}^{(k)}}{\tau_{BK}^{(k)}}, \tag{26}$$

where $m_{BK,\infty}^{(k)}$ and $\tau_{BK}^{(k)}$ are explicit functions of V, directly or via the local Ca^{2+} concentration (see Eq. S36). The probability that k noninactivated CaVs are present in a complex with n CaVs is $\binom{n}{k} h^k (1-h)^{n-k}$, and the whole-cell BK_{Ca} current, is approximated by the following:

$$I_{BK} = g_{BK} \sum_{k=1}^{n} \binom{n}{k} h^k (1-h)^{n-k} m_{BK}^{(k)} (V - V_K), \tag{27}$$

which involves n ODEs (Eq. 26) for the activations variables $m_{BK}^{(k)}$, and one ODE for h ($h = 1 - b$, where b is given by Eq. 20). As shown in Fig. 2 *C*, this expression provides a good approximation to the results from Monte Carlo simulations of the full Markov Chain. Note that if the CaVs do not inactivate, Eq. 27 reduces to the following:

$$I_{BK} = g_{BK} m_{BK}^{(n)} (V - V_K). \tag{28}$$

We can now easily investigate how different stoichiometries of the BK_{Ca}-CaV complexes influence, e.g., activation of the BK_{Ca} channels. As expected, we find that the activation curve is shifted upwards as the number of CaVs per complex increase (Fig. 2 *B*, *upper*). Interestingly, a left shift of the activation curve is seen when n increases. For example, with $n = 4$ CaVs per BK_{Ca} channel, BK_{Ca} activation is half-maximal at $V \approx -14$ mV, compared to $V \approx -5$ mV when $n = 1$, and half-maximal CaV activation at $V \approx -12$ mV. This result is due to the fact that the probability of at least one CaV being open is greater with more channels in the complex. For higher voltages, the single channel current decreases and the CaV open probability increases, with the result that, at strongly positive voltages, BK_{Ca} activation decays more gradually at $n = 1$ than for higher n. This difference is because the local Ca^{2+} level obtained with a single open CaV is insufficient for complete BK_{Ca} activation, and therefore the presence of more CaVs per complex becomes advantageous, because the CaVs may open simultaneously, leading to higher local Ca^{2+} levels. This interpretation also underlies the finding that

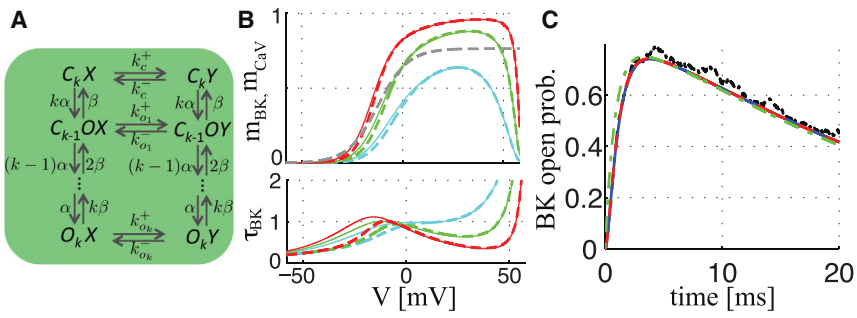

FIGURE 2 Multiple CaVs per BK_{Ca}-CaV complex. (*A*) Shown here is the Markov chain model for complexes with k noninactivated CaVs. (*B*) Shown here are steady-state BK_{Ca} activation functions (*upper*) and time constants (*lower*) for BK_{Ca} channels in complexes with 1 (*cyan*), 2 (*green*), or 4 (*red*) CaVs given from Eq. 26 (see Eq. S36 for the details; *solid*) or from the approximation defined by Eq. 29 (*dashed*). The gray dashed curve shows the CaV activation function $m_{CaV,\infty}$, for comparison. (*C*) Shown here are simulated BK_{Ca} open probabilities in response to a voltage step from −80 to 0 mV, obtained from Monte Carlo simulations of the Markov model of n inactivating independent CaVs controlling a BK_{Ca} channel (*black*), from the ODE model of all states in (*A*) coupled to CaV inactivation (Eq. 27; Eqs. S19–S25; *solid blue*), from the reduced ODE model considering CaV activation kinetics (Eqs. 26 and 27; *dashed red*), and from the simplification assuming $m_{CaV} = m_{CaV,\infty}$ (Eqs. 29 and 27; *dash-dotted green*). To see this figure in color, go online.

BK_{Ca} activation is faster with higher n at positive voltages (Fig. 2 *B*, *lower*).

As mentioned above, many whole-cell models assume instantaneous activation of Ca*Vs*. This assumption implies that vertical transitions in Fig. 2 *A* are in quasi-equilibrium, and hence that, e.g., $p_{C_i O_{k-i} Y} = \binom{k}{i}(1 - m_{CaV,\infty})^{k-i} m_{CaV,\infty}^{i} p_Y$, with notation as for the case of 1:1 stoichiometry. Then, $m_{BK}^{(k)}$ follows Eq. 26 with

$$\tau_{BK}^{(k)} = \left[\sum_{i=1}^{k}\binom{k}{i}(1 - m_{\mathrm{CaV},\infty})^{k-i} m_{\mathrm{CaV},\infty}^{i}\left(k_{o_i}^{+} + k_{o_i}^{-}\right) + (1 - m_{\mathrm{CaV},\infty})^{k} k_c^{-}\right]^{-1},$$
$$m_{BK,\infty}^{(k)} = \left[\sum_{i=1}^{k}\binom{k}{i}(1 - m_{\mathrm{CaV},\infty})^{k-i} m_{\mathrm{CaV},\infty}^{i} k_{o_i}^{+}\right]\tau_{BK}^{(k)}. \quad (29)$$

This simplified expression provides decent fits to activation functions (Fig. 2 *B*, *upper*) and simulated currents (Fig. 2 *C*), and—in our experience—yields reliable results in whole-cell simulations for cells with relatively slow action potential dynamics, as shown below, despite a slight underestimation of $\tau_{BK}^{(k)}$ at negative voltages (Fig. 2 *B*, *lower*).

Whole-cell simulations of electrical activity shaped by BK_{Ca}-CaV complexes

We now illustrate the type of whole-cell modeling that can be performed readily with our Hodgkin-Huxley-type model of the BK_{Ca} current controlled locally by CaVs in BK_{Ca}-CaV complexes.

BK_{Ca}-CaV stoichiometry controls fAHP in a neuronal model

It is well established that in many neurons, BK_{Ca} channels play an important role in action potential (AP) repolarization and fast after-hyperpolarization (fAHP), i.e., the undershoot seen after an AP (2,38), which is important, e.g., for controlling firing frequency and transmitter release. We here adapt a model of AP generation and fAHP in hypothalamic neurosecretory cells (20) to investigate how BK_{Ca}-CaV complexes influence fAHP. In the original model, CaVs are assumed not to inactivate, and to activate instantaneously. We modified the model to include CaV activation dynamics with time constant $\tau_{CaV} = 1.25$ ms (37,39), and inserted our whole-cell BK_{Ca} model (Eq. 28) in place of the original representation of BK_{Ca} currents.

Our results suggest that more than one CaV channel is needed in the BK_{Ca}-CaV complex to develop fAHP that is reduced by BK_{Ca}-channel blockers (Fig. 3 *A*). The difference between 1:1 and 1:*n* BK_{Ca}-CaV stoichiometry is not a simple result of more BK_{Ca} conductance. Increasing the BK_{Ca} conductance fourfold in the case of 1:1 stoichiometry, much more than the difference between the activation functions $m_{BK,\infty}^{(1)}$ and $m_{BK,\infty}^{(4)}$ (Fig. 2 *B*), leads to less fAHP than for 1:4 stoichiometry (Fig. 3 *A*, *inset*). Thus, differences in BK_{Ca} activation kinetics and the shapes of activation functions (Fig. 2 *B*) play a nontrivial role in shaping APs.

Different CaV types affect electrical activity differently in a model of human β-cell electrophysiology

In our recent model of electrical activity in human β-cells (22,23), we modeled the BK_{Ca}-current heuristically. The BK_{Ca} open probability was proportional to the whole-cell Ca^{2+} current, and this expression was found to reasonably reproduce published data (40) regarding the BK_{Ca} activation function and the effects of BK_{Ca} block on AP firing (22).

We now assume that the BK_{Ca} channels form complexes with either T-, L-, or P/Q-type CaVs (22,40), and vary the BK_{Ca}-CaV stoichiometry. As explained in greater detail in the Supporting Material, the different types of CaV differ with respect to activation and inactivation properties, and whole-cell conductance (22,23). The resulting BK_{Ca} model is then fit to experimental I-V data (40) (Fig. S7), and inserted in the whole-cell model. T-type CaVs inactivate rapidly (22,40), and do not activate much BK_{Ca} current during the relatively broad action potentials. For this reason, simulated BK_{Ca} block results in almost no increase in AP height (Fig. 3 *B*), in contrast to experiments (40).

In human β-cells, L-type Ca^{2+} channels show inactivation on a timescale comparable to the duration of an AP (22,40). When coupled to BK_{Ca} channels in the model, good fits to the BK_{Ca} I-V activation curve are obtained, but for different values of the maximal whole-cell BK_{Ca} conductance g_{BK} (Fig. S7). In simulations of electrical activity, BK_{Ca} currents controlled by L-type CaVs reduce AP height, independently of the number of CaVs per complex (Fig. 3 *C*).

BK_{Ca}-CaV complexes with P/Q-type Ca^{2+} channels, which activate at very depolarized potentials and show

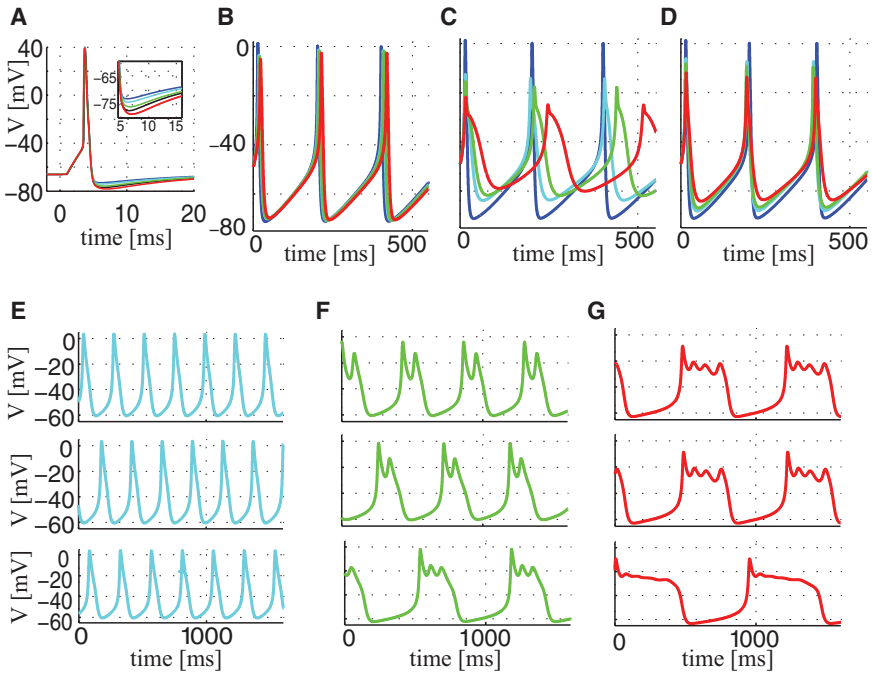

FIGURE 3 Whole-cell simulations. (*A*) Shown here is a simulated AP in a neuronal model (20) with 1:*n* stoichiometry BK_{Ca}-CaV complexes with $n = 1$ (*cyan*), $n = 2$ (*green*), or $n = 4$ (*red*). The whole-cell BK_{Ca} current is described by Eq. 28 (i.e., BK_{Ca} coupled with noninactivating CaVs), where the BK_{Ca} activation, $m_{BK}^{(n)}$, is modeled by Eq. 26 (see Eq. S36 for the details) and $g_{BK} = 1$ mS cm^{-2}. The blue curve shows the case of BK_{Ca} block ($g_{BK} = 0$ mS cm^{-2}), and the trace in black displays the result with $n = 1$, $g_{BK} = 4$ mS cm^{-2}. The inset shows a zoom-in on the fAHP. (*B–D*) Shown here are simulated APs in a model of human β-cells (22) with BK_{Ca} channels located in complexes with n T-type (*B*), L-type (*C*), or P/Q-type (*D*) CaVs, with $n = 1$, 2, or 4. The whole-cell BK_{Ca} current is described by Eq. 27 (with inactivating T- and L-type CaVs) or Eq. 28 (with noninactivating P/Q-type CaVs), where $m_{BK}^{(n)}$ is modeled by Eq. 29. Color coding as in (*A*). (*E–G*) Shown here is simulated activity in a model of lactotrophs (21) with 1:*n* BK_{Ca}-CaV complexes with $n = 1$ (*E*), $n = 2$ (*F*), or $n = 4$ (*G*). The whole-cell BK_{Ca} current is described by Eq. 28, where $m_{BK}^{(n)}$ is modeled by the complete BK_{Ca} model with $2 \times (n + 1)$ states (Fig. 2 *A*) described using Eqs. S19–S25 (*upper traces*), by Eq. 26 (*middle traces*), and by Eq. 29 (*lower traces*). To see this figure in color, go online.

very slow inactivation in human β-cells (22,40), lead to BK_{Ca} currents that activate at slightly more depolarized potentials than in experiments, except for the case of 1:4 BK_{Ca}-CaV stoichiometry (Fig. S7). Simulated application of a BK_{Ca} channel antagonist increases AP height ~15 mV, in good correspondence with experiments. Assuming fewer CaVs per complex, leads to poorer fit of the I-V curve and to less difference between APs obtained with operating and blocked BK_{Ca} channels (Fig. 3 *D*).

We conclude that AP firing is affected differently by BK_{Ca} currents depending on the CaV type controlling BK_{Ca} activity, due to differences in activation and inactivation properties. Because BK_{Ca} block stimulates insulin secretion in human (40) and mouse (41) β-cells, a better understanding of the interaction between different types of CaVs and BK_{Ca} channels may provide novel insight into insulin release in health and disease.

Bursting behavior depends on BK_{Ca}-CaV stoichiometry in a model of pituitary cells

In pituitary cells, BK_{Ca} channels have been found to be intimately involved in the genesis of so-called plateau bursting, which consists of a few small oscillations riding on a depolarized plateau, and is important for secretion (42,43). We now investigate how BK_{Ca}-CaV properties affect such bursting activity in a model of electrical activity in pituitary lactotrophs (21). In this model a single Ca^{2+}-channel type is present, which is assumed to activate instantaneously and not to inactivate. The BK_{Ca} current was modeled as a purely voltage-dependent current, neglecting Ca^{2+} dependency (21). In place of this simplified representation, we substitute our concise BK_{Ca} model controlled by CaVs in complexes.

With 1:1 stoichiometry, spiking electrical activity is observed, because insufficient BK_{Ca} current is generated (Fig. 3 *E*). In contrast, with more than one CaV per complex, plateau bursting appears with the number of small oscillations per burst depending on the number of CaVs per BK_{Ca}-CaV complex (Fig. 3, *F* and *G*). Although the quantitative behavior is independent of the approximation for $m_{BK}^{(n)}$, minor qualitative differences are present. The approximation given by Eq. 26 reproduces very well the behavior obtained from the complete model for the BK_{Ca}-CaV complex (Fig. 3, *F* and *G*, *upper* and *middle panels*), whereas the further simplification given by Eq. 29 produces smaller and more spikes per burst. Nonetheless, considering parameter uncertainties and experimental variations, even Eq. 29 produces reliable results.

DISCUSSION

Models of cellular electrical activity typically do not consider local control in ion channel complexes. This fact is probably to a large extent because of the large computational costs of detailed simulations of Markov chain models (17) or reaction-diffusion models (10) that consider single complexes. In contrast, in the field of Ca^{2+} modeling, global

procedures that respect local mechanisms have been presented (28–30).

We here applied similar methods to the BK_{Ca}-CaV complex to obtain Hodgkin-Huxley representations of the BK_{Ca} current that correctly take local control into account. Importantly, in our approach the effects of ion channel colocalization are handled via a deterministic model representation by averaging the stochastic dynamics in single ion channel complexes appropriately. Our timescale analysis allowed us to handle scenarios with more than one CaV per BK_{Ca}-CaV complex, thus providing important insight into the role of channel stoichiometry. Treating such cases via direct stochastic simulations of the BK_{Ca} and CaV simulations would be computationally cumbersome, and would not provide the same kind of analytical understanding. For example, we found explicit expressions for the time to first opening of a BK_{Ca} channel, thus providing theoretical insight into simulation results (17). Our findings also highlighted that $n > 1$ CaV per complex left shifts the BK_{Ca} activation curve, because the presence of more CaVs increase the probability that at least one CaV is open and activates the associated BK_{Ca} channel.

We illustrated the usefulness of our theoretical results by applying the concise representations of BK_{Ca} currents to previously published whole-cell models of electrical activity. We chose a model of neuronal APs that has previously been used to investigate how BK_{Ca} channels contribute to fAHP (20). The simulations based on our BK_{Ca}-CaV model suggest that the kinetics of BK_{Ca} activation, which depends on the number of associated CaVs (Fig. 2), influence fAHP generation. It would be interesting to investigate experimentally whether defective BK_{Ca}-CaV coupling underlies disturbances in fAHP generation, as predicted by the model. In *Xenopus* motor nerve terminals, BK_{Ca}-CaV coupling differs between the release face and the nonsynaptic surface of varicosities (44), which, in the light of our simulations, may indicate spatial heterogeneity with respect to, e.g., fAHP.

We went on to investigate how the activation and inactivation properties of specific types of Ca^{2+} channels assumed to be present in BK_{Ca}-CaV complexes influence whole-cell electrical activity in a model of human β-cells (22). Because both the coupling of BK_{Ca} channels to L- and P/Q-type CaVs and the different stoichiometries of the complexes allow for simulations comparable to experiments, our findings do not allow us to conclude on the structure of BK_{Ca}-CaV complexes in human β-cells. Further insight into the control by CaVs of BK_{Ca} channels, which are involved in regulation of insulin release (40,41), may lead to a better understanding of β-cell function and how it becomes disturbed in diabetes.

Finally, a model of pituitary cells (21) was used to study the role of BK_{Ca} channels in the generation of plateau bursting, which is important for secretion of pituitary hormones (42). We found that a reduced number of CaVs per complex, for example because of disturbed BK_{Ca}-CaV coupling, may abolish bursting activity. Our simulations showed that even the simplification given by Eq. 29 provided reliable results (Fig. 3, *E–G*). Similar conclusions hold for the β-cell model (see Fig. S7). Interestingly, this was not the case in the neuronal model (20) (Fig. S6), likely because of the shorter neuronal AP being more sensitive to the kinetics of BK_{Ca} activation.

A general strategy to distinguish between different configurations of the BK_{Ca}-CaV complex could be to first estimate the maximal whole-cell BK_{Ca} conductance, for example by depolarizations to highly positive voltages to activate BK_{Ca} channels independently of CaV activity (16), and then to fit I-V curves obtained from voltage-clamp depolarizations (37,40) using the expressions presented here.

In summary, we have presented a concise Hodgkin-Huxley-type model of BK_{Ca} currents that take into account local control in BK_{Ca}-CaV complexes with different stoichiometries. Our model should be useful for whole-cell simulations of electrical activity in neurons and other excitable cells. The approach should be relatively straightforward to apply to other ion channel complexes, e.g., the Cav3-Kv4 complex (45).

SUPPORTING MATERIAL

Supporting Materials and Methods, seven figures, three tables, and one data file are available at http://www.biophysj.org/biophysj/supplemental/S0006-3495(17)30451-4.

AUTHOR CONTRIBUTIONS

All authors performed research, prepared Supporting Material, revised the article, and approved the final version. F.M., A.T., and M.G.P. prepared figures. F.M. developed methods. M.G.P. conceived research and wrote the article.

ACKNOWLEDGMENTS

We thank Carles Rovira, University of Barcelona, for useful discussions during early phases of the work.

REFERENCES

1. Hodgkin, A. L., and A. F. Huxley. 1952. A quantitative description of membrane current and its application to conduction and excitation in nerve. *J. Physiol.* 117:500–544.

2. Berkefeld, H., B. Fakler, and U. Schulte. 2010. Ca^{2+}-activated K^+ channels: from protein complexes to function. *Physiol. Rev.* 90:1437–1459.

3. Pallotta, B. S., K. L. Magleby, and J. N. Barrett. 1981. Single channel recordings of Ca^{2+}-activated K^+ currents in rat muscle cell culture. *Nature.* 293:471–474.

4. Barrett, J. N., K. L. Magleby, and B. S. Pallotta. 1982. Properties of single calcium-activated potassium channels in cultured rat muscle. *J. Physiol.* 331:211–230.

5. Cox, D. H., J. Cui, and R. W. Aldrich. 1997. Allosteric gating of a large conductance Ca-activated K^+ channel. *J. Gen. Physiol.* 110:257–281.
6. Latorre, R., and S. Brauchi. 2006. Large conductance Ca^{2+}-activated K^+ (BK) channel: activation by Ca^{2+} and voltage. *Biol. Res.* 39:385–401.
7. Grunnet, M., and W. A. Kaufmann. 2004. Coassembly of big conductance Ca^{2+}-activated K^+ channels and L-type voltage-gated Ca^{2+} channels in rat brain. *J. Biol. Chem.* 279:36445–36453.
8. Berkefeld, H., C. A. Sailer, …, B. Fakler. 2006. BK_{Ca}-Cav channel complexes mediate rapid and localized Ca^{2+}-activated K^+ signaling. *Science.* 314:615–620.
9. Müller, A., M. Kukley, …, D. Dietrich. 2007. Nanodomains of single Ca^{2+} channels contribute to action potential repolarization in cortical neurons. *J. Neurosci.* 27:483–495.
10. Rehak, R., T. M. Bartoletti, …, G. W. Zamponi. 2013. Low voltage activation of KCa1.1 current by Cav3-KCa1.1 complexes. *PLoS One.* 8:e61844.
11. Suzuki, Y., H. Yamamura, …, Y. Imaizumi. 2013. Caveolin-1 facilitates the direct coupling between large conductance Ca^{2+}-activated K^+ (BK_{Ca}) and Cav1.2 Ca^{2+} channels and their clustering to regulate membrane excitability in vascular myocytes. *J. Biol. Chem.* 288:36750–36761.
12. Chad, J. E., and R. Eckert. 1984. Calcium domains associated with individual channels can account for anomalous voltage relations of CA-dependent responses. *Biophys. J.* 45:993–999.
13. Simon, S. M., and R. R. Llinás. 1985. Compartmentalization of the submembrane calcium activity during calcium influx and its significance in transmitter release. *Biophys. J.* 48:485–498.
14. Neher, E. 1998. Vesicle pools and Ca^{2+} microdomains: new tools for understanding their roles in neurotransmitter release. *Neuron.* 20:389–399.
15. Fakler, B., and J. P. Adelman. 2008. Control of K_{Ca} channels by calcium nano/microdomains. *Neuron.* 59:873–881.
16. Berkefeld, H., and B. Fakler. 2013. Ligand-gating by Ca^{2+} is rate limiting for physiological operation of BK_{Ca} channels. *J. Neurosci.* 33:7358–7367.
17. Cox, D. H. 2014. Modeling a Ca^{2+} channel/BK_{Ca} channel complex at the single-complex level. *Biophys. J.* 107:2797–2814.
18. Stanley, D. A., B. L. Bardakjian, …, W. L. Ditto. 2011. Stochastic amplification of calcium-activated potassium currents in Ca^{2+} microdomains. *J. Comput. Neurosci.* 31:647–666.
19. Anwar, H., I. Hepburn, …, E. De Schutter. 2013. Stochastic calcium mechanisms cause dendritic calcium spike variability. *J. Neurosci.* 33:15848–15867.
20. Roper, P., J. Callaway, …, W. Armstrong. 2003. AHP's, HAP's and DAP's: how potassium currents regulate the excitability of rat supraoptic neurones. *J. Comput. Neurosci.* 15:367–389.
21. Tabak, J., N. Toporikova, …, R. Bertram. 2007. Low dose of dopamine may stimulate prolactin secretion by increasing fast potassium currents. *J. Comput. Neurosci.* 22:211–222.
22. Pedersen, M. G. 2010. A biophysical model of electrical activity in human β-cells. *Biophys. J.* 99:3200–3207.
23. Riz, M., M. Braun, and M. G. Pedersen. 2014. Mathematical modeling of heterogeneous electrophysiological responses in human β-cells. *PLOS Comput. Biol.* 10:e1003389.
24. Khaliq, Z. M., N. W. Gouwens, and I. M. Raman. 2003. The contribution of resurgent sodium current to high-frequency firing in Purkinje neurons: an experimental and modeling study. *J. Neurosci.* 23:4899–4912.
25. Jaffe, D. B., B. Wang, and R. Brenner. 2011. Shaping of action potentials by type I and type II large-conductance Ca^{2+}-activated K^+ channels. *Neuroscience.* 192:205–218.
26. Anwar, H., S. Hong, and E. De Schutter. 2012. Controlling Ca^{2+}-activated K^+ channels with models of Ca^{2+} buffering in Purkinje cells. *Cerebellum.* 11:681–693.
27. Sherman, A., J. Keizer, and J. Rinzel. 1990. Domain model for Ca^{2+}-inactivation of Ca^{2+} channels at low channel density. *Biophys. J.* 58:985–995.
28. Hinch, R., J. L. Greenstein, …, R. L. Winslow. 2004. A simplified local control model of calcium-induced calcium release in cardiac ventricular myocytes. *Biophys. J.* 87:3723–3736.
29. Greenstein, J. L., R. Hinch, and R. L. Winslow. 2006. Mechanisms of excitation-contraction coupling in an integrative model of the cardiac ventricular myocyte. *Biophys. J.* 90:77–91.
30. Williams, G. S. B., M. A. Huertas, …, G. D. Smith. 2007. A probability density approach to modeling local control of calcium-induced calcium release in cardiac myocytes. *Biophys. J.* 92:2311–2328.
31. Lobo, F. G., and D. E. Goldberg. 1997. Decision making in a hybrid genetic algorithm. *In* IEEE International Conference on Evolutionary Computation. Institute of Electrical and Electronics Engineers, Indianapolis, IN, pp. 121–125.
32. Fleming, P. J., and R. C. Purshouse. 2002. Evolutionary algorithms in control systems engineering: a survey. *Control Eng. Pract.* 10:1223–1241.
33. Neher, E. 1998. Usefulness and limitations of linear approximations to the understanding of Ca^{++} signals. *Cell Calcium.* 24:345–357.
34. Marcantoni, A., D. H. F. Vandael, …, E. Carbone. 2010. Loss of Cav1.3 channels reveals the critical role of L-type and BK channel coupling in pacemaking mouse adrenal chromaffin cells. *J. Neurosci.* 30:491–504.
35. Buchholz, P., J. Kriege, and I. Felko. 2014. Input modeling with phase-type distributions and Markov models. *In* Springer Briefs in Mathematics. Springer, Berlin, Germany http://dx.doi.org/10.1007/978-3-319-06674-5.
36. Segel, L. A., and M. Slemrod. 1989. The quasi steady-state assumption: a case study in perturbation. *SIAM Rev.* 31:446–477.
37. Berkefeld, H., and B. Fakler. 2008. Repolarizing responses of BK_{Ca}-Cav complexes are distinctly shaped by their Cav subunits. *J. Neurosci.* 28:8238–8245.
38. Storm, J. F. 1987. Action potential repolarization and a fast after-hyperpolarization in rat hippocampal pyramidal cells. *J. Physiol.* 385:733–759.
39. Joux, N., V. Chevaleyre, …, N. Hussy. 2001. High voltage-activated Ca^{2+} currents in rat supraoptic neurones: biophysical properties and expression of the various channel α1 subunits. *J. Neuroendocrinol.* 13:638–649.
40. Braun, M., R. Ramracheya, …, P. Rorsman. 2008. Voltage-gated ion channels in human pancreatic β-cells: electrophysiological characterization and role in insulin secretion. *Diabetes.* 57:1618–1628.
41. Houamed, K. M., I. R. Sweet, and L. S. Satin. 2010. BK channels mediate a novel ionic mechanism that regulates glucose-dependent electrical activity and insulin secretion in mouse pancreatic β-cells. *J. Physiol.* 588:3511–3523.
42. Stojilkovic, S. S., H. Zemkova, and F. Van Goor. 2005. Biophysical basis of pituitary cell type-specific Ca^{2+} signaling-secretion coupling. *Trends Endocrinol. Metab.* 16:152–159.
43. Tagliavini, A., J. Tabak, …, M. G. Pedersen. 2016. Is bursting more effective than spiking in evoking pituitary hormone secretion? A spatiotemporal simulation study of calcium and granule dynamics. *Am. J. Physiol. Endocrinol. Metab.* 310:E515–E525.
44. Sun, X.-P., B. Yazejian, and A. D. Grinnell. 2004. Electrophysiological properties of BK channels in *Xenopus* motor nerve terminals. *J. Physiol.* 557:207–228.
45. Anderson, D., W. H. Mehaffey, …, R. W. Turner. 2010. Regulation of neuronal activity by Cav3-Kv4 channel signaling complexes. *Nat. Neurosci.* 13:333–337.

Biophysical Journal, Volume *112*

Supplemental Information

Concise Whole-Cell Modeling of BK_{Ca}-CaV Activity Controlled by Local Coupling and Stoichiometry

Francesco Montefusco, Alessia Tagliavini, Marco Ferrante, and Morten Gram Pedersen

Supporting Material

Concise whole-cell modeling of $BK_{Ca}CaV$ activity controlled by local coupling and stoichiometry

F Montefusco, A Tagliavini, M Ferrante, M Pedersen

List of contents

1 Model of the 1:1 BK_{Ca}-CaV complex

First, we justify the product formulation for the voltage and Ca^{2+}-dependent rate constants k^- and k^+ (Eqs. 2 and 3 in the main text). We assume (i) that, for fixed Ca^{2+} concentration (Ca), BK_{Ca} activity is described by a Boltzmann function, and (ii) that the slope parameter of the Boltzmann function is independent of Ca, a reasonable assumption for Ca^{2+} concentrations above 1 μM (1–3) as expected in BK_{Ca}-CaV complexes (2, 4). Based on assumption (i), we express the rate constants by the standard expressions

$$k^-(V,Ca) = \tilde{w}^-(Ca)e^{-w_{yx}(Ca)V}, \quad k^+(V,Ca) = \tilde{w}^+(Ca)e^{-w_{xy}(Ca)V}.$$

The open fraction of BK_{Ca} channels is then

$$p_{Y_\infty} = \frac{k^+(V,Ca)}{k^-(V,Ca)+k^+(V,Ca)} = \frac{1}{1-e^{-\frac{V-V_0(Ca)}{S_0(Ca)}}},$$

where we have highlighted that in principal V_0 and S_0 depend on Ca. In particular the slope parameter is given by

$$S_0(Ca) = \frac{1}{w_{yx}(Ca)-w_{xy}(Ca)},$$

and from assumption (ii) we obtain that $w_{xy}(Ca)$ is equal to $w_{yx}(Ca)$ except from a constant independent of Ca. We make the simplifying assumption that also w_{yx} and w_{xy} are independent of Ca. Finally, writing

$$\tilde{w}^-(Ca) = w_0^- f^-(Ca), \quad \tilde{w}^+(Ca) = w_0^+ f^+(Ca)$$

we obtain Eqs. 2-5 in the main text.

We couple the two state (closed and open) model for the BK_{Ca} channel (see Methods, Table S1 reporting the optimal model parameters, and Figure S1 showing a representation of the model and the fits to the data) with the three state (closed, open and inactivated or blocked) model for the CaV channel (see Methods and Table S1). Figure 1A in the main text shows a cartoon of the model of the 1:1 BK_{Ca}-CaV complex, where CX, OX and BX correspond to the closed state for the BK_{Ca} channel (X) coupled with the closed (C), open (O) and inactivated (B) states for the CaV, respectively, and CY, OY and BY correspond to the open state for the BK_{Ca} channel (Y) coupled with the closed (C), open (O) and inactivated (B) states for the CaV, respectively.

The parameters k_c^- and k_o^- (k_c^+ and k_o^+) are defined by Eq. 2 (Eq. 3) of the main text with Ca equal to Ca_c and Ca_o, respectively. Ca_c is the concentration at the BK_{Ca} channel when the associated CaV is closed (or inactivated, i.e. $Ca_c = Ca_b$) and is set equal to 0.2 μM (background Ca^{2+} concentration). Ca_o is the concentration at the BK_{Ca} channel when the CaV is open and is given by

$$Ca_o = \frac{i_{Ca}}{8\pi r D_{Ca} F} \exp\left[\frac{-r}{\sqrt{\frac{D_{Ca}}{k_B^+[B_{total}]}}}\right], \tag{S1}$$

where $i_{Ca} = \bar{g}_{Ca}(V - V_{Ca})$ is the single-channel Ca^{2+} current, and $r = 13$ nm the distance between CaV and BK_{Ca} channels (2, 4). At $V = 0$ mV, $Ca_o \approx 19$ μM. Other parameters are given in Table S2 (2). Note that for the parameters used here (Table S1), $k_c^+ \approx 0$ (i.e., the probability of BK_{Ca} opening when the CaV is closed is practically zero).

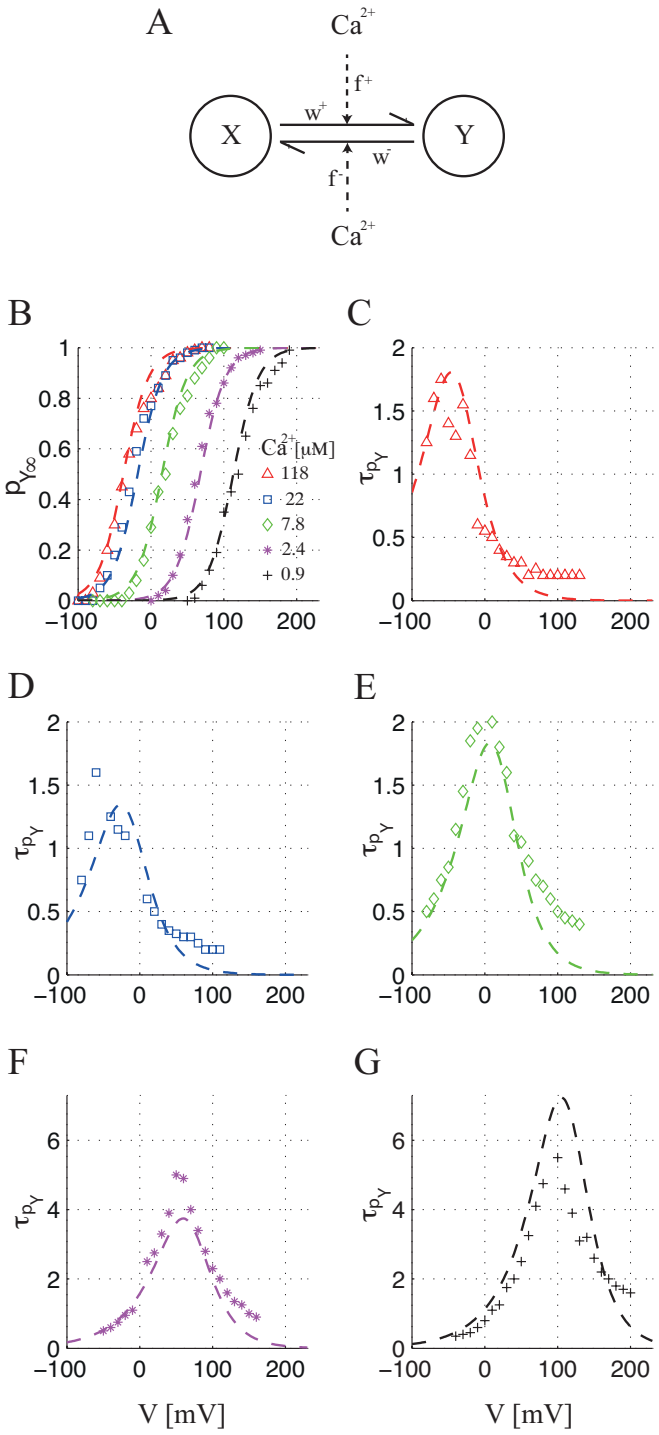

Figure S1: **BK_{Ca} channel model: fit to the data.** **(A)** Schematic representation of the model, where X and Y indicate the closed and open states of the BK_{Ca} channel. **(B)** Steady-state BK_{Ca} open probabilities vs. voltage at different Ca^{2+}concentrations (different markers for different Ca^{2+} levels as indicated in the legend) and the corresponding fit obtained by the model (dashed lines). **(C)-(G)** Time constants (in ms) vs. voltage data at given Ca^{2+}concentrations (see legend in panel B), and the corresponding model fits (dashed lines).

Table S1: **Optimal model parameters for the BK_{Ca}-CaV complex.**

BK_{Ca} channel model described by Eq. 1 of the main text		
Parameter	Value	Unit
w_0^-	3.32	ms^{-1}
w_0^+	1.11	ms^{-1}
w_{yx}	0.022	mV^{-1}
w_{xy}	−0.036	mV^{-1}
K_{yx}	0.1	μM
K_{xy}	16.6	μM
n_{yx}	0.46	-
n_{xy}	2.33	-
CaV activation described by Eqs. 16 and 17 of the main text		
Parameter	Value	Unit
α_0	1.2979	ms^{-1}
α_1	−0.0639	mV^{-1}
β_0	1.0665	ms^{-1}
β_1	0.0703	mV^{-1}
ρ	0.309	-

Table S2: **Parameters for calculating Ca^{2+} at the BK_{Ca} channel taken from (2)**.

Parameter	Value	Unit
r	13	nm
D_{Ca}	250	$\mu m^2\ s^{-1}$
F	9.6485	C mol^{-1}
k_B	500	$\mu M^{-1}\ s^{-1}$
B_{total}	30	μM
V_{Ca}	60	mV
$\bar{g}_{Ca}$	2.8	pS

1.1 Monte Carlo Simulations

We perform Monte Carlo simulations for the devised complex in order to model its stochastic gating. Initially the CaV and BK_{Ca} channels are closed. Then, for both the channels, the transitions from one state (closed, open or inactivated for CaV, closed or open for BK_{Ca}) to the others are given by the procedure explained below. First, we define the transition matrices for the CaV,

$$\begin{aligned} Q_{CaV} &= \begin{bmatrix} P[C,t+\Delta t|C,t] & P[C,t+\Delta t|O,t] & 0 \\ P[O,t+\Delta t|C,t] & P[O,t+\Delta t|O,t] & P[O,t+\Delta t|B,t] \\ 0 & P[B,t+\Delta t|O,t] & P[B,t+\Delta t|B,t] \end{bmatrix} \\ &= \begin{bmatrix} 1-\alpha\Delta t & \beta\Delta t & 0 \\ \alpha\Delta t & 1-\beta\Delta t-\delta\Delta t & \gamma\Delta t \\ 0 & \delta\Delta t & 1-\gamma\Delta t \end{bmatrix}, \end{aligned} \tag{S2}$$

and for the BK channel,

$$\begin{aligned} Q_{BK_{Ca}} &= \begin{bmatrix} P[X,t+\Delta t|X,t] & P[X,t+\Delta t|Y,t] \\ P[Y,t+\Delta t|X,t] & P[Y,t+\Delta t|Y,t] \end{bmatrix} \\ &= \begin{bmatrix} 1-k^+\Delta t & k^-\Delta t \\ k^+\Delta t & 1-k^-\Delta t \end{bmatrix} \end{aligned} \tag{S3}$$

where the elements correspond to the transition probabilities between the indicated states in the time interval $[t, t+\Delta t]$, provided that Δt is small.

At any time point, we compute the state of the BK_{Ca}-CaV complex according the following procedure. We choose a random number ξ uniformly distributed on the interval $[0,1]$ for the CaV channel, and make a transition based upon the subinterval in which ξ falls. For example, if the CaV channel is open (O) (see the second column of Q_{CaV} defined by Eq. S2), it remains open if $\xi < 1-\beta\Delta t-\delta\Delta t$, while a transition to the inactivated (B) state occurs if $\xi \geq 1-\beta\Delta t-\delta\Delta t$ and $\xi < 1-\beta\Delta t$, otherwise ($\xi \geq 1-\beta\Delta t$ and $\xi \leq 1$) a transition to the closed (C) state occurs. Similarly, we choose a random number η uniformly distributed on the interval $[0,1]$ for the BK_{Ca} channel, and make a transition based upon the subinterval in which η falls. Note that the Ca^{2+} concentration for the BK_{Ca} channel at any time point is determined by the state of the CaV channel. This procedure is repeated for every time point to achieve the Monte Carlo simulations. We used $\Delta t = 0.01$ ms. Smaller time steps were checked and gave identical results.

1.2 Time to first opening and phase-type distributions

The continuous-time Markov chain Z in Figure 1A in the main text takes values in the state space $S = \{CX, OX, BX,\ BY, CY, OY\}$. We denote its initial distribution by λ and its generating matrix by Q, where

$$Q = \begin{bmatrix} -\alpha-k_c^+ & \alpha & 0 & 0 & k_c^+ & 0 \\ \beta & -\beta-\delta-k_o^+ & \delta & 0 & 0 & k_o^+ \\ 0 & \gamma & -\gamma-k_c^+ & k_c^+ & 0 & 0 \\ 0 & 0 & k_c^- & -\gamma-k_c^- & 0 & \gamma \\ k_c^- & 0 & 0 & 0 & -\alpha-k_c^- & \alpha \\ 0 & k_o^- & 0 & \delta & \beta & -\beta-\delta-k_o^- \end{bmatrix}.$$

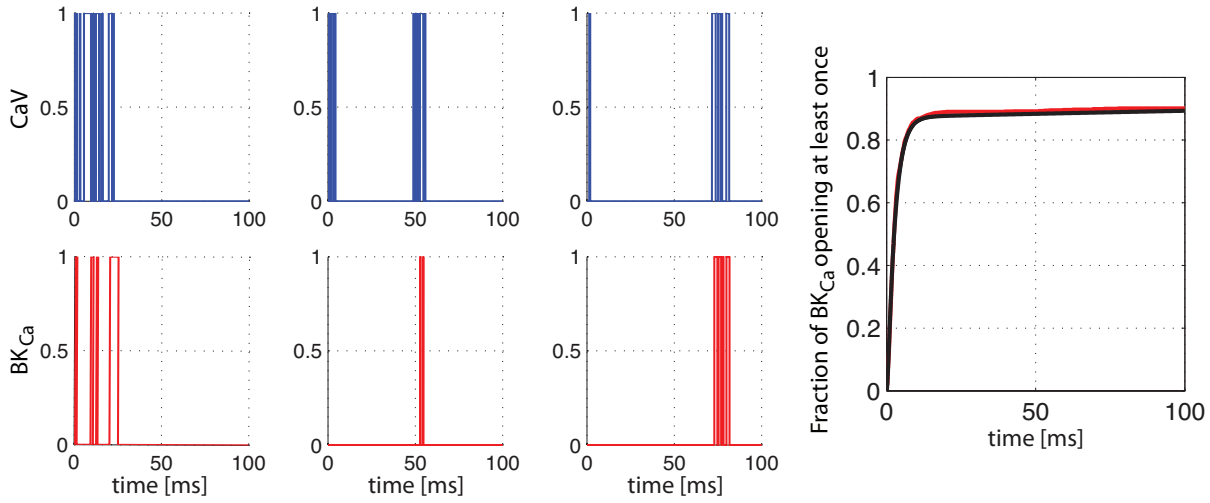

Figure S2: **Time to first opening for the 1:1 BK_{Ca}-CaV complex**. Left: Three Markov chain realizations for the 1:1 BK_{Ca}-CaV complex. Right: The empirical fraction of BK_{Ca} channels that exhibit the first channel opening before t (red) and the theoretical expression $P(T_{CX,Y} < t)$ (black) from Eq. 22 of the main text. Note that in the second and third examples of Markov chain realizations, the CaV inactivates early before the BK_{Ca} channel opens, and only later when the CaV reactivates (at ∼50 ms and ∼70 ms) does the BK_{Ca} open for the first time. Such cases cause the late, slowly rising phase in the right panel, whereas the more typical case where the BK_{Ca} channel opens early (as in the first example shown on the left) creates the rapid early rise in the right panel.

Assuming that $k_c^+ = 0$, the generating matrix Q become

$$Q = \begin{bmatrix} -\alpha & \alpha & 0 & 0 & 0 & 0 \\ \beta & -\beta-\delta-k_o^+ & \delta & 0 & 0 & k_o^+ \\ 0 & \gamma & -\gamma & 0 & 0 & 0 \\ 0 & 0 & k_c^- & -\gamma-k_c^- & 0 & \gamma \\ k_c^- & 0 & 0 & 0 & -\alpha-k_c^- & \alpha \\ 0 & k_o^- & 0 & \delta & \beta & -\beta-\delta-k_o^- \end{bmatrix}. \tag{S4}$$

Define the random variable

$$H = \inf\{t \geq 0 : Z_t \in \{CY, OY, BY\}\}, \tag{S5}$$

i.e., the (random) time to first opening, which can be described with phase-type distribution theory (5). We are interested in evaluating its conditional distribution and expectation, given that $Z_0 = CX$, i.e., with the initial distribution $\lambda = (1, 0, 0, 0, 0, 0)$. Defined $S_0 = \{CX, OX, BX, BY, CY\}$ and the matrix $\overline{Q} = (q_{i,j})_{i,j \in S_0}$, a simple application of phase-type distribution theory yields Eqs. 21 and 22 of the main text, as shown in "Time to first opening" in the Results section. Figure S2 shows that the simulated first opening times are well described by Eq. 22 of the main text.

2 Time-scale analysis and model simplifications

2.1 ODE model of the 1:1 BK_{Ca}-CaV complex

The deterministic description of the complex, corresponding to the Markov Chain described above, is given by the following ODE system

$$\frac{dp_{CX}}{dt} = k_c^- p_{CY} + \beta p_{OX} - (k_c^+ + \alpha) p_{CX}, \tag{S6}$$

$$\frac{dp_{CY}}{dt} = k_c^+ p_{CX} + \beta p_{OY} - (k_c^- + \alpha) p_{CY}, \tag{S7}$$

$$\frac{dp_{OX}}{dt} = k_o^- p_{OY} + \alpha p_{CX} + \gamma p_{BX} - (k_o^+ + \beta + \delta) p_{OX}, \tag{S8}$$

$$\frac{dp_{OY}}{dt} = k_o^+ p_{OX} + \alpha p_{CY} + \gamma p_{BY} - (k_o^- + \beta + \delta) p_{OY}, \tag{S9}$$

$$\frac{dp_{BX}}{dt} = k_c^- p_{BY} + \delta p_{OX} - (k_c^+ + \gamma) p_{BX}, \tag{S10}$$

$$\frac{dp_{BY}}{dt} = k_c^+ p_{BX} + \delta p_{OY} - (k_c^- + \gamma) p_{BY}, \tag{S11}$$

where p_Z, with $Z \in \{CX, CY, OX, OY, BX, BY\}$, represents the probability of the complex to be in one of the six states of the model. Then $p_Y = p_{CY} + p_{OY} + p_{BY}$. In the following, we assume $k_c^+ = 0$.

2.2 Model simplification

As explained in the Results section, since re- and inactivation of CaVs are slower than (de-)activation, the ODE model defined by Eqs. S6–S11 can be split into two submodels with respectively 4 and 2 states (the green and blue boxes in Figure 1A in the main text). Then, by considering only the activation of the BK_{Ca}-CaV complexes with non-inactivated CaV, and exploiting the relations $p_{CY} + p_{OY} = m_{BK}$, $p_{OX} + p_{OY} = m_{CaV}$, and $p_{CX} + p_{CY} = 1 - m_{CaV}$, where m_{BK} and m_{CaV} are the BK_{Ca} and the CaV activation variables, respectively, BK_{Ca} activation can be modeled by the two following ODEs,

$$\frac{dp_{CY}}{dt} = \beta m_{BK} - (k_c^- + \alpha + \beta) p_{CY}, \tag{S12}$$

$$\frac{dm_{BK}}{dt} = m_{CaV} k_o^+ + \left(k_o^+ + k_o^- + \alpha + \beta\right) p_{CY} - (k_o^+ + k_o^- + \beta) m_{BK}, \tag{S13}$$

with m_{CaV} modeled by Eq. 18 of the main text. Assuming quasi-steady state for p_{CY} ($\frac{dp_{CY}}{dt} \approx 0$) then yields

$$p_{CY} = \frac{\beta}{k_c^- + \alpha + \beta} m_{BK}. \tag{S14}$$

By substituting Eq. S14 into Eq. S13, we achieve a single ODE describing the dynamics of BK_{Ca} activation in complexes with non-inactivated CaV,

$$\frac{dm_{BK}}{dt} = m_{CaV} k_o^+ - \frac{(k_o^+ + k_o^-)(k_c^- + \alpha) + \beta k_c^-}{\alpha + \beta + k_c^-} m_{BK}. \tag{S15}$$

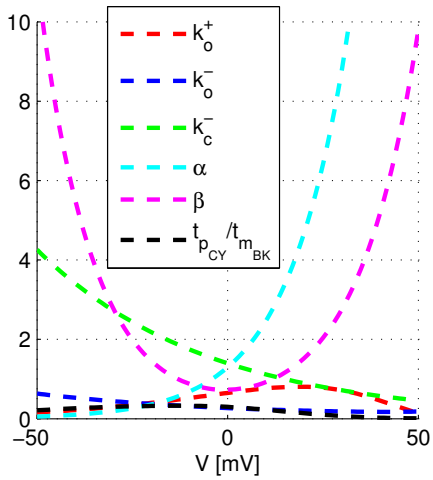

Figure S3: **Time scale analysis for the 1:1 BK_{Ca}-CaV complex**. Model parameters as function of voltage, showing that the transitions described by α, β and k_c^- are the fastest. This fact leads to a separation of time scales, as shown by the black curve illustrating $t_{p_{CY}}/t_{m_{BK}}$ in Eq. S18, which is always less than 0.33, and for most voltages considerably smaller.

Therefore, the equilibrium open fraction of the BK_{Ca} channels in complexes with non-inactivated CaV, $m_{BK,\infty}$, and the corresponding time constant, τ_{BK}, are given as in Eq. 24 of the main text.

Coupling the one state model for the BK_{Ca} activation (Eq. S15) with the inactivation of the CaV channel allows us to reproduce the dynamics of the BK_{Ca}-CaV complex described by Eqs. S6–S11 and the corresponding Monte Carlo simulations (see Figure 1 in the main text). In particular, the open probability of the BK_{Ca} channel, $p_Y = p_{CY} + p_{OY} + p_{BY}$, can be described by

$$p_Y \approx m_{BK} h, \tag{S16}$$

where h is the fraction of non-inactivated CaV (see Eqs. 15 and 20 of the main text).

2.3 Time scale analysis

For a more formal analysis, we follow (6). The quasi-steady state approximation for p_{CY} is valid when the time scales of the two variables in question differ, i.e., $t_{p_{CY}} \ll t_{m_{BK}}$, where $t_{m_{BK}}$ is the time scale of changes m_{BK} after an initial (fast) transient, i.e., when the approximation is consistent (6). The (fast) time scale for p_{CY} is given from Eq. S12, assuming that m_{BK} is constant, as

$$t_{p_{CY}} = \frac{1}{\alpha + \beta + k_c^-} \ . \tag{S17}$$

The (slow) time scale for m_{BK} is given as the time scale of m_{BK} assuming that the quasi-steady state approximation holds, i.e., $t_{m_{BK}} = \tau_{BK}$ in Eq. 24 of the main text. Then

$$\frac{t_{p_{CY}}}{t_{m_{BK}}} = \frac{(k_o^- + k_o^+)(k_c^- + \alpha) + \beta k_c^-}{(\alpha + \beta + k_c^-)^2}, \tag{S18}$$

which is small (Figure S3).

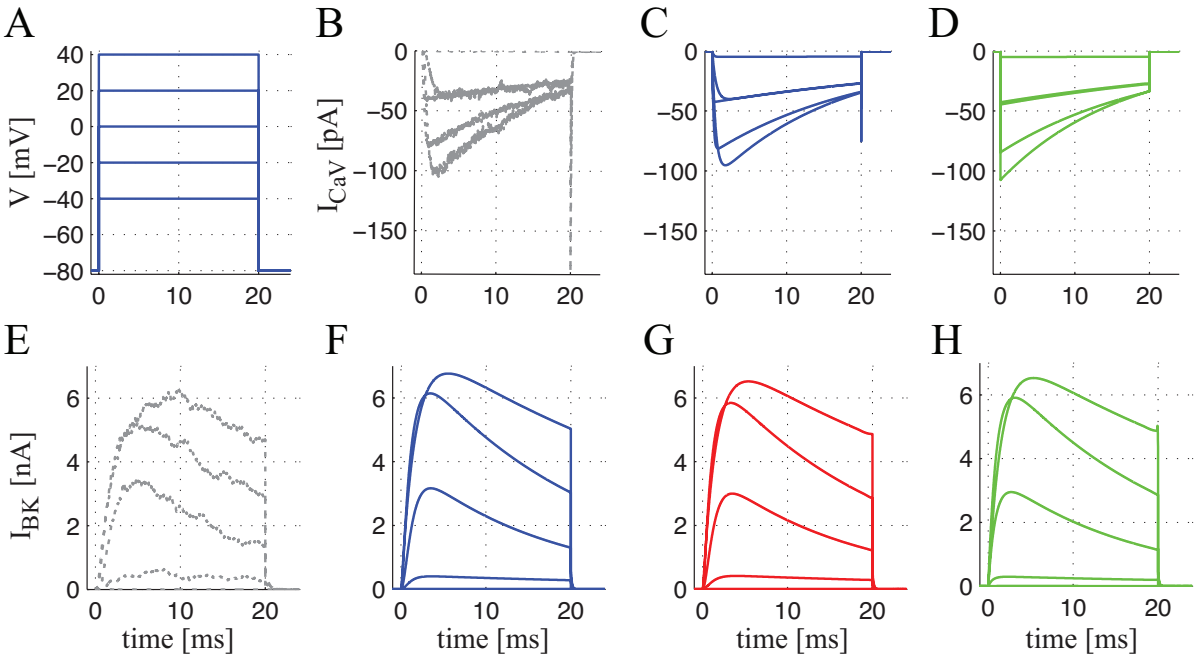

Figure S4: **Model responses to different voltage steps for the 1:1 BK_{Ca}-CaV complex.** **(A)** Voltage steps from -80 mV to from -40 mV to 40 mV in 20 mV increments for 20 ms and then back to -80 mV. Simulated CaV currents in response to the different voltage steps obtained from **(B)** the 7-state Markov chain model (see (2); gray), **(C)** the ODE model corresponding to the 3-state Markov chain model (Eqs. 13-15 of the main text; blue), and **(D)** the corresponding model assuming instantaneous activation $m_{CaV} = m_{CaV,\infty}$ (Eq. 20 of the main text; green). Simulated BK_{Ca} currents in response to the different voltage steps obtained from **(E)** the original 70-state Markov chain model (see (2); gray), **(F)** the ODE model corresponding to the 6-state Markov chain model (Eqs. S19–S24; blue), **(G)** the simplified Hodgkin-Huxley-type model (Eq. 25 of the main text; red), and **(H)** the corresponding model assuming instantaneous activation $m_{CaV} = m_{CaV,\infty}$ (green; see main text). Each trace is the sum of 1000 single complex responses.

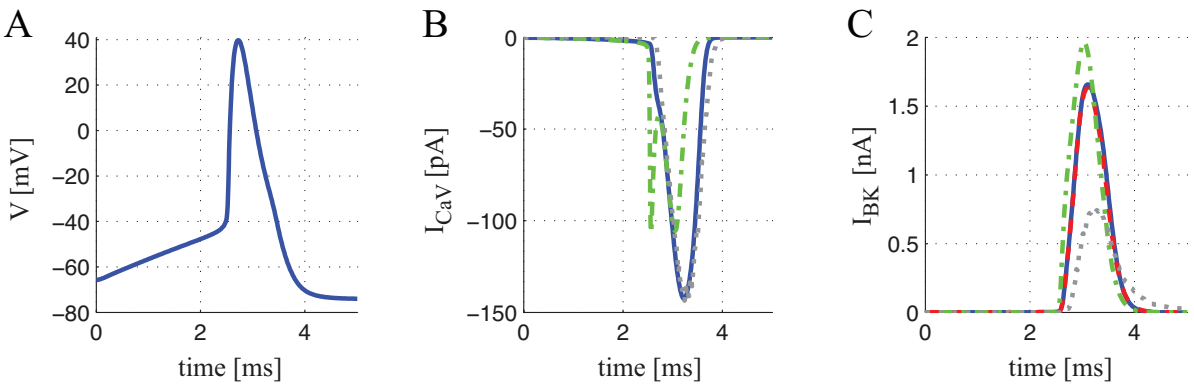

Figure S5: **Model responses to a simulated AP generated by a model of hypothalamic neurosecretory cells (7). (A)** Simulated AP. **(B)** Simulated CaV currents in response to the simulated AP obtained from the 7-state Markov chain model ((2); dotted gray), the ODE model corresponding to the 3-state Markov chain model (Eqs. 13-15 of the main text; solid blue), and the corresponding model assuming instantaneous activation $m_{CaV} = m_{CaV,\infty}$ (Eq. 20 of the main text; dash-dotted green). **(C)** Simulated BK_{Ca} currents in response to the simulated AP obtained from the original 70-state Markov chain model ((2); gray), the ODE model corresponding to the 6-state Markov chain model (Eqs. S19–S24; solid blue), the simplified Hodgkin-Huxley-type model (Eq. 25 of the main text; dashed red), and the corresponding model assuming instantaneous activation $m_{CaV} = m_{CaV,\infty}$ (dash-dotted green; see main text). Each trace is the sum of 1000 single complex responses.

2.4 Responses of the 1:1 BK_{Ca}-CaV complex to voltage steps and AP

Figure S4 shows the current response of the 1:1 BK_{Ca}-CaV complex to different step voltages (Figure S4A). The whole-cell CaV current for the 3-state ODE model ($I_{CaV} = N_{CaV}\bar{g}_{Ca}m_{CaV}h$, where $N_{CaV} = 1000$ is the number of CaV channels, $\bar{g}_{Ca}$ is defined in Table S2 and m_{CaV} and h are given by Eqs. 13-18 of the main text) approximates the 7-state Markov chain model (2) current very well for each step voltage (Figure S4BC). Also, the further simplification for the 3-state ODE model assuming instantaneous activation of the CaV currents ($m_{CaV} = m_{CaV,\infty}$, green plots in Figure S4D) provides a good approximation of the Monte Carlo simulations. The whole-cell BK_{Ca} current for our simplified 6-state Markov chain model ($I_{BK} = N_{BK}\bar{g}_{BK}p_Y$, where $N_{BK} = 1000$ is the number of BK_{Ca} channels, $\bar{g}_{BK} = 100$ pF is the single BK_{Ca} channel conductance (8) and p_Y is given by Eqs. S19-S24) approximates the 70-state Markov chain model (2) current very well for each step voltage (Figure S4EF). Moreover, our simplified Hodgkin-Huxley-type model current for the BK_{Ca} channel (Eq. 25 of the main text; red plots in Figure S4G), and the corresponding model assuming instantaneous activation of the CaV currents (green plots in Figure S4H) also works very well.

Figure S5 shows the current response of the 1:1 BK_{Ca}-CaV complex to a simulated action potential (AP) generated by a model of hypothalamic neurosecretory cells (7) (Figure S5A). As for the voltage step response case, the whole-cell CaV current for the 3-state ODE model approximates the 7-state Markov chain model current very well (see solid blue and dotted gray plots in Figure S5B). However, the further simplification for the 3-state ODE model assuming instantaneous activation of the CaV currents (dash-dotted green plot in Figure S5B) determines an additional early peak of current and a faster decay. For the whole-cell BK_{Ca} current, the peak obtained from the 70-state Markov chain model is lower than that obtained from our simplified

models (Figure S5C). This discrepancy is likely due to an overestimation of the BK_{Ca} activation time constant of BK_{Ca} model devised by Cox (2) at specific Ca_o (compare the left lower panel of Figure 2D in (2) with Figure S1D, where $Ca_o = 22$ μM). The slower time constant prevents complete activation of the BK_{Ca} channels for Cox' 70-state Markov chain model during the imposed AP.

3 Model for BK_{Ca} activation in complexes with k non-inactivated CaVs and its approximation

For the case of 1:n BK_{Ca}-CaV stoichiometry, we split the system according to the number k of non-inactivated CaV channels. Then the equivalent 1:k BK_{Ca}-CaV complex can be described by the following ODE system:

$$\frac{dp_{C_kX}}{dt} = \beta p_{C_{k-1}OX} + k_c^- p_{C_kY} - (k\alpha + k_c^+) p_{C_kX} \tag{S19}$$

$$\frac{dp_{C_kY}}{dt} = \beta p_{C_{n-1}OY} + k_c^+ p_{C_nX} - (k\alpha + k_c^-) p_{C_nY} \tag{S20}$$

$$\begin{aligned}\frac{dp_{C_{k-i}O_iX}}{dt} &= (i+1)\beta p_{C_{k-(i+1)}O_{i+1}X} + (k-(i-1))\alpha p_{C_{k-(i-1)}O_{i-1}X} \\ &\quad + k_{oi}^- p_{C_{k-i}O_iY} - ((k-i)\alpha + i\beta + k_{oi}^+) p_{C_{k-i}O_iX}, \quad i = 1, \ldots, k-1\end{aligned} \tag{S21}$$

$$\begin{aligned}\frac{dp_{C_{k-i}O_iY}}{dt} &= (i+1)\beta p_{C_{n-(i+1)}O_{i+1}Y} + (k-(i-1))\alpha p_{C_{k-(i-1)}O_{i-1}Y} \\ &\quad + k_{oi}^+ p_{C_{k-i}O_iX} - ((k-i)\alpha + i\beta + k_{oi}^-) p_{C_{k-i}O_iY}, \quad i = 1, \ldots, k-1\end{aligned} \tag{S22}$$

$$\frac{dp_{O_kX}}{dt} = \alpha p_{CO_{k-1}X} + k_{ok}^- p_{O_kY} - (k\beta + k_{ok}^+) p_{O_kX} \tag{S23}$$

$$\frac{dp_{O_kY}}{dt} = \alpha p_{CO_{k-1}Y} + k_{ok}^+ p_{O_kX} - (k\beta + k_{ok}^-) p_{O_kY} \tag{S24}$$

where, e.g., $p_{C_{k-i}O_iX}$ and $p_{C_{k-i}O_iY}$ correspond to the probability of having $k-i$ closed and i open CaVs coupled with the closed (X) and open (Y) BK_{Ca} channel, respectively. The activation of the BK_{Ca} surrounded by k non-inactivated CaVs, $m_{BK}^{(k)}$, is then

$$m_{BK}^{(k)} = p_{C_kY} + \sum_{i=1}^{k-1} p_{C_{k-i}O_iY} + p_{O_kY}. \tag{S25}$$

By taking into account that

$$p_{C_kX} = (1 - m_{CaV})^k - p_{C_kY} \tag{S26}$$

$$p_{C_{k-i}O_iX} = \binom{k}{i} (1 - m_{CaV})^{k-i} m_{CaV}^i - p_{C_{k-i}O_iY}, \quad i = 1, \ldots, k-1 \tag{S27}$$

$$p_{O_kX} = m_{CaV}^k - p_{O_kY} \tag{S28}$$

and renaming the state variables as follows

$$\begin{aligned} p_{Y_0} &= p_{C_kY} && \text{(S29)}\\ p_{Y_1} &= p_{C_{k-1}O_Y} + p_{Y_0} && \text{(S30)}\\ &\vdots \\ p_{Y_i} &= p_{C_{k-i}O_iY} + p_{Y_{i-1}} && \text{(S31)}\\ &\vdots \\ m_{BK}^{(k)} = p_{Y_k} &= p_{O_kY} + p_{Y_{k-1}} && \text{(S32)} \end{aligned}$$

we can reduce the ODE system from $2(k+1)$ to $(k+1)$ equations.

Moreover, assuming the quasi-steady state approximation for p_{Y_i}, with $i = 0, \ldots, k-1$,

$$\frac{dp_{Y_i}}{dt} = 0,$$

then

$$\begin{aligned} p_{Y_0} &= A_1 p_{Y_1} + D_1 && \text{(S33)}\\ &\vdots \\ p_{Y_i} &= A_{i+1} p_{Y_{i+1}} + D_{i+1} && \text{(S34)}\\ &\vdots \\ p_{Y_{k-1}} &= A_k m_{BK}^{(k)} + D_n && \text{(S35)} \end{aligned}$$

where (for brevity, $m = m_{CaV}$)

$$\begin{aligned} A_1 =& \frac{\beta}{k\alpha + \beta + k_c^- + k_c^+} \cong \frac{\beta}{k\alpha + \beta + k_c^-}\\ D_1 =& \frac{k_c^+ (1-m)^k}{k\alpha + \beta + k_c^- + k_c^+} \cong 0\\ A_i =& \frac{i\beta}{B_i}, \qquad i = 2, \ldots, k\\ D_i =& \left(\sum_{j=1}^{i-1} \binom{k}{j} (1-m)^{k-j} m^j - k_c^- \left(D_1 + \sum_{j=2}^{i-1} D_j \left(\prod_{l=1}^{j-1} A_l \right) \right) \right) / B_i\\ & \left(- \sum_{j=1}^{i-2} \left(k_{oj}^+ + k_{oj}^- \right) \left((1 - A_j) \left(D_{j+1} + \sum_{l=j+2}^{i-1} D_l \left(\prod_{m=j+1}^{l-1} A_m \right) \right) - D_j \right) \right) / B_i\\ & \left(+ \left((k - (i-1))\, \alpha + k_{o(i-1)}^+ + k_{o(i-1)}^- \right) D_{i-1} \right) / B_i, \quad i = 2, \ldots, k \end{aligned}$$

with

$$\begin{aligned} B_i =& \left((k - (i-1))\, \alpha + k_{o(i-1)}^+ + k_{o(i-1)}^- \right) (1 - A_{i-1}) + i\beta + k_c^- \left(\prod_{j=1}^{i-1} A_j \right)\\ & + \sum_{j=1}^{i-2} \left(k_{oj}^+ + k_{oj}^- \right) (1 - A_j) \left(\prod_{l=j+1}^{i-1} A_l \right), \quad i = 2, \ldots, k. \end{aligned}$$

Then

$$
\begin{aligned}
p_{Y_i} &= \left(\prod_{j=1}^{k} A_j\right) m_{BK}^{(k)} + D_{i+1} + \sum_{j=i+2}^{k} D_j \left(\prod_{l=i}^{j-1} A_l\right),\ i = 0, \ldots, k-1 \\
p_{C_k Y} &= \left(\prod_{j=1}^{k} A_j\right) m_{BK}^{(k)} + D_1 + \sum_{j=2}^{k} D_j \left(\prod_{l=1}^{j-1} A_l\right) \\
p_{C_{k-i}O_iY} &= (1 - A_i) \left(\prod_{j=i+1}^{k} A_j\right) m_{BK}^{(k)} + (1 - A_i) \left(D_{i+1} + \sum_{j=i+2}^{k} D_j \left(\prod_{l=i+1}^{j-1} A_l\right)\right) \\
&\quad - D_i, \quad i = 1, \ldots, k-1 \\
p_{O_k Y} &= (1 - A_k)\, m_{BK}^{(k)} - D_k.
\end{aligned}
$$

Finally, we achieve one ODE for describing the dynamics of the $\mathrm{BK_{Ca}}$ activation with k non-inactivated CaVs:

$$
\begin{aligned}
\frac{dm_{BK}^{(k)}}{dt} &= \sum_{i=1}^{k} \binom{k}{i} (1-m)^{k-i} m^i k_{oi}^{+} - k_c^{-} p_{C_k Y} - \sum_{i=1}^{k} \left(k_{oj}^{+} + k_{oj}^{-}\right) p_{C_{k-i}O_iY} \\
&= \left\{ \sum_{i=1}^{k} \binom{k}{i} (1-m)^{k-i} m^i k_{oi}^{+} - k_c^{-} \left(D_1 + \sum_{j=2}^{k} D_j \left(\prod_{l=1}^{j-1} A_l\right)\right) \right. \\
&\quad - \sum_{i=1}^{k-1} \left(k_{oj}^{+} + k_{oj}^{-}\right) \left((1 - A_i) \left(D_{i+1} + \sum_{j=i+2}^{k} D_j \left(\prod_{l=i+1}^{j-1} A_l\right)\right) - D_i\right) \\
&\quad \left. + \left(k_{ok}^{+} + k_{ok}^{-}\right) D_n \right\} \qquad \text{(S36)} \\
&\quad - \left[\left(k_{ok}^{+} + k_{ok}^{-}\right) (1 - A_k) + k_c^{-} \prod_{j=1}^{k} A_j + \sum_{i=1}^{k-1} \left(k_{oj}^{+} + k_{oj}^{-}\right) (1 - A_i) \prod_{j=i+1}^{k} A_j \right] m_{BK}^{(k)}.
\end{aligned}
$$

Therefore, the activation time constant of the $\mathrm{BK_{Ca}}$ channels in complexes with k non-inactivated CaVs, $\tau_{BK}^{(k)}$, is the inverse of the expression in square brackets in Eq. S36, whereas the $\mathrm{BK_{Ca}}$ equilibrium open fraction, $m_{BK,\infty}^{(k)}$, is equal to the product of $\tau_{BK}^{(k)}$ and the expression in curly brackets. Note that $\tau_{BK}^{(k)}$ depends only on parameters, whereas $m_{BK}^{(k)}$ depends also on m_{CaV} via D_i.

If assuming instantaneous activation of CaVs, we have

$$
p_{C_{k-i}O_iY} = \binom{k}{i} (1 - m_{CaV,\infty})^{k-i} m_{CaV,\infty}^{i} p_Y, \quad i = 0, \ldots, k,
$$

and (cf. Eq. 29 of the main text)

$$\begin{aligned}\frac{dm_{BK}^{(k)}}{dt} &= \sum_{i=1}^{k}\binom{k}{i}(1-m_{CaV,\infty})^{n-i}m_{CaV,\infty}^{i}k_{io}^{+} - k_{c}^{-}p_{C_kY} - \sum_{i=1}^{k}\left(k_{oj}^{+}+k_{oj}^{-}\right)p_{C_{k-i}O_iY} \\ &= \sum_{i=1}^{k}\binom{k}{i}(1-m_{CaV,\infty})^{k-i}m_{CaV,\infty}^{i}k_{oi}^{+} \\ &\quad - \left((1-m_{CaV,\infty})^{k}k_{c}^{-} + \sum_{i=1}^{k}\binom{k}{i}(1-m_{CaV,\infty})^{k-i}m_{CaV,\infty}^{i}\left(k_{oi}^{+}+k_{oi}^{-}\right)\right)m_{BK}.\end{aligned} \tag{S37}$$

4 Whole-cell models

4.1 Hypothalamic neuronal model

We extended a model of electrical activity in hypothalamic neurosecretory cells (7) with our devised BK_{Ca}-CaV model. The model is described by

$$\frac{dV}{dt} = -\frac{1}{C}\left(I_{BK} + I_{SK} + I_K + I_A + I_{Na} + I_{Ca} + I_{leak}\right). \tag{S38}$$

where I_{BK} and I_{SK} represent the calcium- and voltage-dependent K^+ currents carried by BK and SK channels, respectively; I_K and I_A denote the delayed rectifier and the A-current respectively; I_{Na} represents the sodium current and I_{Ca} the calcium current. C is the membrane capacitance and is equal to 1 μF cm^{-2}.

We modified the calcium current and inserted our whole-cell BK_{Ca} model in place of the original representation of BK_{Ca} currents. In particular, according to experimental data (9, 10), we introduced CaV activation dynamics, whereas the original model assumed instantaneous activation of CaVs, and modified the equilibrium voltage-dependent activation. Then

$$I_{Ca} = g_{Ca}m_{CaV}(V - V_{Ca}) \tag{S39}$$

where g_{Ca} and V_{Ca} are the maximal whole-cell conductance and the Ca^{2+} reverse potential, respectively (7). m_{CaV} is defined by Eq. 18 of the main text, with $\tau_{CaV} = 1.25$ ms. For the equilibrium voltage-dependent activation, given in (7) and defined by $m_{CaV,\infty} = \left(1 + e^{\frac{-V-V_m}{k_m}}\right)^{-1}$, we modified the V_m parameter of the Boltzmann function ($V_m = 15$ mV).

The I_{BK} current is modeled by Eq. 28 of the main text, where the BK_{Ca} activation, $m_{BK}^{(n)}$, is given by Eq. 26. Moreover, we also considered the case where the activation of the BK_{Ca} channel is given by the complete ODE model described by Eqs. S19–S25, and the case where the BK_{Ca} activation is simplified by assuming instantaneous activation of CaVs (see Eq. S37 and Eq. 29 of the main text).

The other currents are expressed as (7)

$$I_{SK} = g_{SK}q_{\infty}^{2}(V - V_K), \tag{S40}$$

$$I_K = g_K m_K^3(V - V_K), \tag{S41}$$

$$I_A = g_A m_A^4 h_A(V - V_K), \tag{S42}$$

$$I_{Na} = g_{Na}[m_{Na,\infty}(V)]^3\, h_{Na}\,(V - V_{Na}), \tag{S43}$$

$$I_{leak} = g_{leak}(V - V_{leak}), \tag{S44}$$

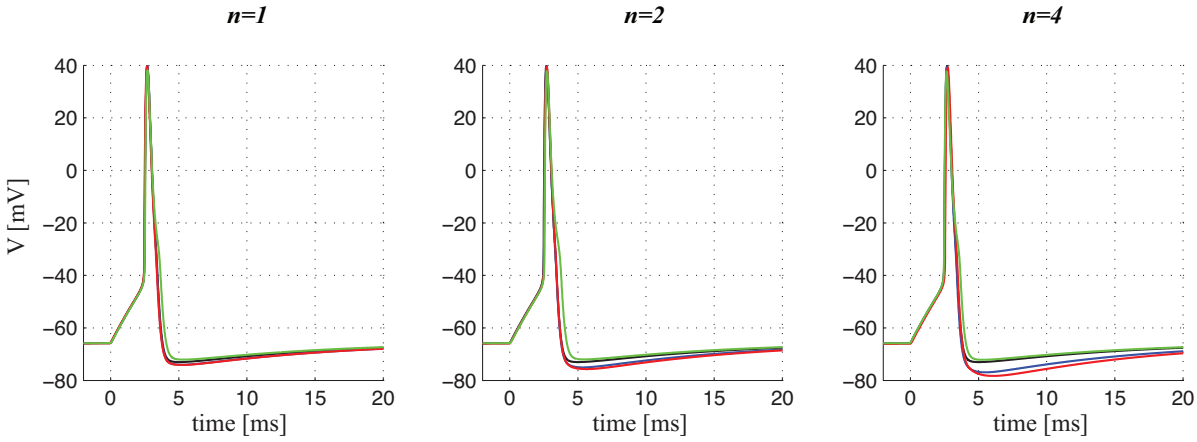

Figure S6: **Whole-cell simulations for the neuronal model (7) with the devised BK_{Ca}-CaV model**. Simulated APs with the BK_{Ca} channels coupled in complexes with n non-inactivating CaVs ($n = 1$, left panel; $n = 2$, middle; $n = 4$, right). In each panel, the whole-cell BK_{Ca} current is described by Eq. 28 of the main text (i.e. BK_{Ca} coupled with non-inactivating CaVs), where the BK_{Ca} activation, $m_{BK}^{(n)}$, is modeled by the full ODE model described by Eqs. S19–S25 (blue curve), by Eq. 26 (see Eq. S36 for the details) (red curve), and by Eq. 29 (green curve), and $g_{BK} = 1$ mS cm^{-2}. The black curve shows the case of BK_{Ca} block ($g_{BK} = 0$ mS cm^{-2}).

where the voltage-dependent activation variables, m_X (and similarly inactivation variabels, h_X, where X denotes the type of current), follow

$$\frac{dm_X}{dt} = \frac{m_{X,\infty}(V) - m_X}{\tau_{mX}}, \tag{S45}$$

where τ_{mX} (respectively τ_{hX}) is the time-constant of activation (respectively inactivation for h_X), and $m_{X,\infty}(V)$ (respectively $h_{X,\infty}(V)$) is the steady-state voltage-dependent activation (respectively inactivation) of the current, described with Boltzmann function. g_X represents the whole-cell conductance of the channel X and V_X the reverse potential. q_∞ is the calcium-dependent activation function for I_{SK} (see Appendix in (7) for parameter values).

Figure S6 shows the simulated AP in this neuronal model with 1:n stoichiometry BK_{Ca}-CaV complexes, where $n = 1$, 2 or 4. The BK_{Ca} activation is modeled by the complete ODE system described by Eqs. S19–S25, by Eq. 26 of the main text, or by Eq. 29. The simplified model (Eq. 29) is not able to reproduce the fast after-hyperpolarization (fAHP), whereas the other two models, which take CaV activation dynamics into account, show how increasing the number of CaVs coupled with BK_{Ca} helps to generate fAHP. The difference associated with the choice of the BK_{Ca} model suggests that the neuronal model is sensitive to the kinetics of BK_{Ca} activation.

4.2 Human β-cell model

The human β-cell model (11) is as follows. The membrane potential is described by

$$\frac{dV}{dt} = -(I_{BK} + I_{Kv} + I_{HERG} + I_{Na} + I_{CaL} + I_{CaPQ} + I_{CaT} + I_{KATP} + I_{leak}), \tag{S46}$$

where the BK_{Ca} current I_{BK} is modeled assuming that BK_{Ca} channels are located in complexes with either T-type, L-type or P/Q-type Ca^{2+} channels. In particular, I_{BK} is described by Eq. 27 of the main text (with inactivating T- and L-type CaVs) or Eq. 28 (with non-inactivating P/Q-type CaVs), where the BK_{Ca} activation, $m_{BK}^{(n)}$, is modeled by Eqs. S19–S25 (full model), Eq. 26, or Eq. 29 (instantaneous CaV activation). As shown in Figure S7, the model is quite robust to the choice of BK_{Ca}-CaV model.

The other currents are

$$I_{Kv} = g_{Kv} m_{Kv} (V - V_K), \tag{S47}$$
$$I_{HERG} = g_{HERG} m_{HERG} h_{HERG} (V - V_K), \tag{S48}$$
$$I_{Na} = g_{Na} m_{Na,\infty}(V) h_{Na} (V - V_{Na}), \tag{S49}$$
$$I_{CaL} = g_{CaL} m_{CaL,\infty}(V) h_{CaL} (V - V_{Ca}), \tag{S50}$$
$$I_{CaPQ} = g_{CaPQ} m_{CaPQ,\infty}(V) (V - V_{Ca}), \tag{S51}$$
$$I_{CaT} = g_{CaT} m_{CaT,\infty}(V) h_{CaT} (V - V_{Ca}), \tag{S52}$$
$$I_{K(ATP)} = g_{K(ATP)} (V - V_K), \tag{S53}$$
$$I_{leak} = g_{leak} (V - V_{leak}), \tag{S54}$$

where activation variables (and similarly inactivations variabels, h_X, where X denotes the type of current) follow

$$\frac{dm_X}{dt} = \frac{m_{X,\infty}(V) - m_X}{\tau_{mX}}, \tag{S55}$$

where τ_{mX} (respectively τ_{hX}) is the time-constant of activation (respectively inactivation for h_X), and $m_{X,\infty}(V)$ (respectively $h_{X,\infty}(V)$) is the steady-state voltage-dependent activation (respectively inactivation) of the current. The steady-state activation (and inactivation) functions are described with Boltzmann functions,

$$m_{X,\infty}(V) = \frac{1}{1 + \exp((V - V_{mX})/n_{mX})}, \tag{S56}$$

except

$$h_{CaL,\infty}(V) = \max\left(0, \min\left\{1, 1 + [m_{CaL,\infty}(V)(V - V_{Ca})]/57\text{mV}\right\}\right), \tag{S57}$$

for Ca^{2+}-dependent inactivation of L-type Ca^{2+} channels. The time-constant for activation of Kv-channes is assumed to be voltage-dependent (11, 12),

$$\tau_{mKv} = \begin{cases} \tau_{mKv,0} + 10 \exp\left(\frac{-20\text{ mV} - V}{6\text{mV}}\right)\text{ ms}, & \text{for } V \geq 26.6\text{ mV}, \\ \tau_{mKv,0} + 30\text{ ms}, & \text{for } V < 26.6\text{ mV}. \end{cases} \tag{S58}$$

We refer to the original paper (11) for details regarding modeling of the different currents.

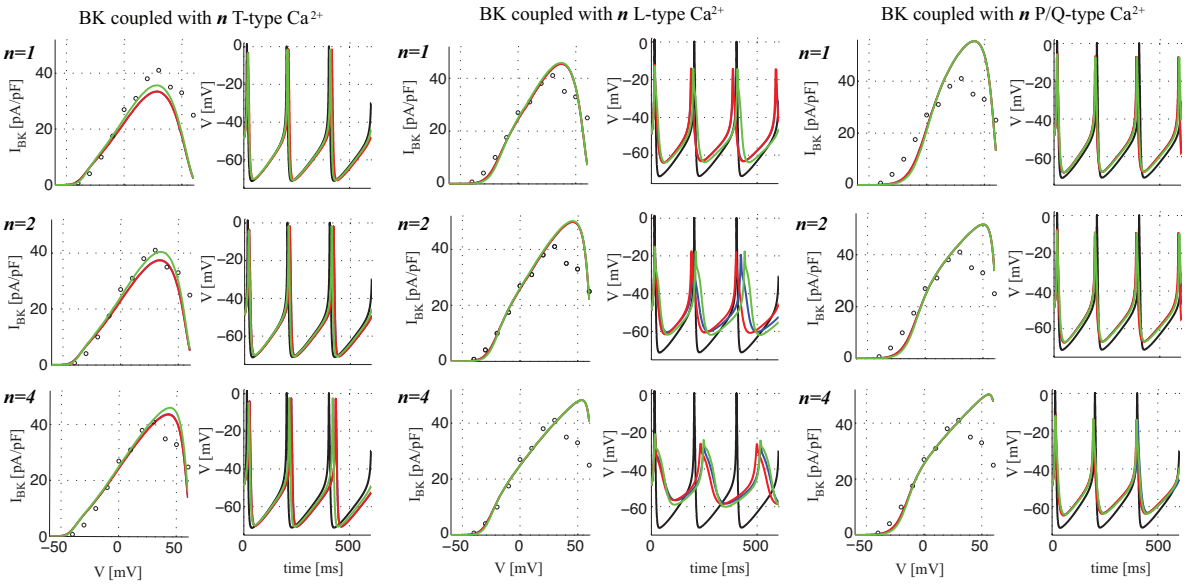

Figure S7: **Whole-cell simulations for the human β-cell model (11) with the devised $\mathbf{BK_{Ca}}$-CaV model.** Simulated APs with BK_{Ca} channels located in complexes with n T-type (left panels), L-type (middle), or P/Q-type (right) CaVs ($n = 1$, upper panels; $n = 2$, middle; $n = 4$, lower). The β-cell model shows little sensitivity to the choice of BK_{Ca}-CaV model. In each panel, the whole-cell BK_{Ca} current is described by Eq. 27 of the main text (with inactivating T- and L-type CaVs) or Eq. 28 (with non-inactivating P/Q-type CaVs), where the BK_{Ca} activation, $m_{BK}^{(n)}$, is modeled by the full ODE model described by Eqs. S19–S25 (blue curve), by Eq. 26 (see Eq. S36 for the details) (red curve), and by Eq. 29 (green curve). Left subpanels show fit to data from (12), right subpanels report model simulations. The black traces show simulations with BK_{Ca} block.

4.3 Pituitary lactotroph model

We extended a pituitary lactotroph model (13) with our concise Hodgkin-Huxley-type model of the BK_{Ca}-CaV complex (Eq. 28 of the main text). The original model includes a single Ca^{2+} current (I_{Ca}), a delayed-rectifier K^+ current (I_K), a Ca^{2+}-gated SK current (I_{SK}), and a leak current (I_{leak}), in addition to the BK current. The membrane potential V evolves in time according to

$$C\frac{dV}{dt} = -(I_{Ca} + I_K + I_{SK} + I_{BK} + I_{leak}), \tag{S59}$$

where C is the membrane capacitance. The currents are modeled as

$$\begin{aligned} I_{Ca} &= g_{Ca} m_{CaV,\infty}(V)(V - V_{Ca}), && \text{(S60)} \\ I_K &= g_K n(V - V_K), && \text{(S61)} \\ I_{SK} &= g_{SK} s_\infty([Ca])(V - V_K), && \text{(S62)} \\ I_{leak} &= g_l(V - V_l), && \text{(S63)} \\ I_{BK} &= g_{BK} m_{BK}^{(n)}(V - V_K), && \text{(S64)} \end{aligned}$$

where the activation variable of the delayed rectifier is given by

$$\frac{dn}{dt} = \frac{n_\infty(V) - n}{\tau_n}. \tag{S65}$$

The equilibrium functions are described as

$$\begin{aligned} m_{CaV,\infty}(V) &= [1 + \exp((v_m - V)/s_m)]^{-1}, && \text{(S66)} \\ n_\infty(V) &= [1 + \exp((v_n - V)/s_n)]^{-1}, && \text{(S67)} \\ s_\infty([Ca]) &= \frac{[Ca]^2}{[Ca]^2 + k_s^2}. && \text{(S68)} \end{aligned}$$

The differential equation for the cytosolic Ca^{2+} concentration is

$$\frac{d[Ca]}{dt} = -f_c(\alpha I_{Ca} + k_c[Ca]). \tag{S69}$$

Table S3 reports the parameter values of the pituitary model (13).

Table S3: **Parameter values of the pituitary model (13)**.

Parameter	Value	Unit
C	10	pF
g_{Ca}	2	nS
V_{Ca}	60	mV
v_m	-20	mV
s_m	12	mV
g_k	3	nS
V_k	-75	mV
v_n	-5	mV
s_n	10	mV
g_{SK}	1.2	nS
k_s	0.4	μM
g_{BK}	1	nS
g_l	0.2	nS
V_l	-50	mV
f_c	0.01	-
α	0.0015	μM fC^{-1}
k_c	0.12	ms^{-1}

Supporting References

1. Cox, D. H., J. Cui, and R. W. Aldrich, 1997. Allosteric gating of a large conductance Ca-activated K+ channel. *J Gen Physiol* 110:257–81.

2. Cox, D. H., 2014. Modeling a Ca(2+) channel/BKCa channel complex at the single-complex level. *Biophys J* 107:2797–814.

3. Latorre, R., and S. Brauchi, 2006. Large conductance Ca2+-activated K+ (BK) channel: activation by Ca2+ and voltage. *Biol Res* 39:385–401.

4. Berkefeld, H., B. Fakler, and U. Schulte, 2010. Ca2+-activated K+ channels: from protein complexes to function. *Physiol Rev* 90:1437–59.

5. Buchholz, P., J. Kriege, and I. Felko, 2014. Input modeling with phase-type distributions and Markov models. Springer Briefs in Mathematics. Springer. `http://dx.doi.org/10.1007/978-3-319-06674-5`.

6. Segel, L. A., and M. Slemrod, 1989. The quasi steady-state assumption: a case study in perturbation. *SIAM Rev.* 31:446–477.

7. Roper, P., J. Callaway, T. Shevchenko, R. Teruyama, and W. Armstrong, 2003. AHP's, HAP's and DAP's: how potassium currents regulate the excitability of rat supraoptic neurones. *J Comput Neurosci* 15:367–89.

8. Pallotta, B. S., K. L. Magleby, and J. N. Barrett, 1981. Single channel recordings of Ca2+-activated K+ currents in rat muscle cell culture. *Nature* 293:471–4.

9. Joux, N., V. Chevaleyre, G. Alonso, L. Boissin-Agasse, F. C. Moos, M. G. Desarménien, and N. Hussy, 2001. High voltage-activated Ca2+ currents in rat supraoptic neurones: biophysical properties and expression of the various channel alpha1 subunits. *J Neuroendocrinol* 13:638–49.

10. Berkefeld, H., and B. Fakler, 2008. Repolarizing responses of BKCa-Cav complexes are distinctly shaped by their Cav subunits. *J Neurosci* 28:8238–45.

11. Pedersen, M. G., 2010. A biophysical model of electrical activity in human β-cells. *Biophys J* 99:3200–3207. `http://dx.doi.org/10.1016/j.bpj.2010.09.004`.

12. Braun, M., R. Ramracheya, M. Bengtsson, Q. Zhang, J. Karanauskaite, C. Partridge, P. R. Johnson, and P. Rorsman, 2008. Voltage-gated ion channels in human pancreatic beta-cells: electrophysiological characterization and role in insulin secretion. *Diabetes* 57:1618–1628. `http://dx.doi.org/10.2337/db07-0991`.

13. Tabak, J., N. Toporikova, M. E. Freeman, and R. Bertram, 2007. Low dose of dopamine may stimulate prolactin secretion by increasing fast potassium currents. *J Comput Neurosci* 22:211–22.